Physics

SCIENCE OF LIGHT

VOLUME 2 NUMBER 1

August
1952

OHIO STATE
UNIVERSITY
NOV 17 1955
LIBRARY

Published by the

Institute for Optical Research

Tokyo University of Education

SCIENCE OF LIGHT

Science of Light contains reports of the Institute for Optical Research and contributions from other science bodies about similar subject.

The editorial staff consists of following members:

Prof. Yoshio Fujioka (Chairman)

Prof. Shoji Kojima

Prof. Tatsuoki Miyajima

Prof. Yoshio Tanaka

Prof. Morikazu Toda

Prof. Shin-ichiro Tomonaga

All communications should be addressed to the director or to the librarian of the Institute.

The Institute for Optical Research

Tokyo University of Education

400, 4-chome, Hyakunin-machi, Sinjuku-ku, Tokyo. Japan

Printed by SANYOSHA PRINTING Co., TOKYO

CONTENTS

Endeavour on Ruling Grating in Japan ..... Y. FUJIOKA, Y .SAKAYANAGI, AND T. KITAYAMA 1

A New Mounting of Concave Grating Suitable for a Spectrometer ..... M. SEYA 8

Construction of a Far Inrfa-Red Spectrometer with Echelette Grating ..... H. YOSHINAGA, AND Y. YAMADA 18

Constrution of a Small Betatron ..... M. MIWA, S. KAGEYAMA, K. FUJII AND K. KURIYAMA 29

Pulse Shape of a Slow Counter ..... R. ITO 37

A Cathode-Ray Investigation of Thin Films of Tin, Zinc, and Cadmium Deposited on a Silver Crystal Face ..... Y. WATANABE 61

On the Absorption Spectrum in the $1s\sigma\, 3p\pi\ {}^1\Pi_{cd} \leftarrow (1s\sigma)^2\ {}^1\Sigma_g^+$ System of the Hydrogen Molecule ..... T. NAMIOKA 73

Band Spectra of Nitric Oxide in the Visible and Near Infra-Red Regions ..... M. OGAWA 87

On the O_2 Atmospheric Bands Appearing in the Emission Spectrum ..... M. SHIMAZU 95

On the PbS Photoconductive Cell ..... N. SASSA AND M. NAKAMURA 104

On the Interference Filter ..... M. IWATA 116

A Hard and Efficient Reflection-Reducing Coating ..... T. SAWAKI AND H. KUBOTA 128

Odour, as a Problem of Physics ..... Y. FUJIOKA 135

Etudes Spectrochimiques des Complexes Métalliques du Troponoïde I ..... T. UÈMURA, AND S. MIYAKAWA 146

Exchange

Endeavour on Ruling Grating in Japan

Yoshio FUJIOKA, Yoshimi SAKAYANAGI
Institute for Optical Research, Tokyo University of Education
and Toshio KITAYAMA
The Scientific Research Institute, Ltd.

(Received December 21, 1951)

About 30 years ago, work to construct a ruling engine for grating was begun in the Institute of Physical and Chemical Research, but later this work was interrupted. We rebegan this work about ten years ago, and recently we have gradually begun to get some result. Although our machine can not be compared with recent machines in America, we can still make gratings capable enough for practical use.

1 Introduction

Since the optical diffraction grating was first completed satisfactorily by Rowland, it has been widely used in pure and applied spectroscopy, also in astronomy. The practical technics to make it are, however, so difficult that it is made at only a few places on the world. If it should be made in our country, it would have to be a great merit for the development of science there.

At the early stage of development of physics in Japan, a plan for making such a grating was enthusiastically looked for by Japanese scientists, and when the Institute of Physical and Chemical Research was built in Tokyo in 1916, the late Professor Nagaoka realized this desire. He sent M. Ono, a young mechanical technician, to the University of Chicago to learn the technics of Michelson's ruling engine. After coming back to Japan, Ono made roughly a skeleton of the main screw and the containing bed of the machine, which then were kept in a cellar for several years to undergo natural aging.

In 1929, another mechanical technician S. Kobayashi, who had entered the Institute, began the construction of a ruling machine in collaboration with Ono. Although they utilized the best technics as they could at that time, they were still unable to use any special device besides usual mechanical technics. The machine accomplished by them had so noticeable an error that it was too difficult to correct it in spite of hard work covering several years. After three years they had to stop their efforts on this work.

In 1942, Fujioka (one of the author), of position in the Institute, thought it regrettable that such a valuable machine had not been used for a long time, and asked two young physicists Kitayama (one of the authors) and Shida, to work on the ruling of gratings. Thus we began the reconstruction of the machine in the time of the 2nd World War. In the war time there were many difficulties for such a long-lasting work. In 1945 we had to remove the machine to a sea-

shore to avoid the bombing, but a part of the machine left in Tokyo was damaged when the Institute was fire-bombed. After much trouble we began again in 1946 the adjustment at a constant temperature room of the Institute in Tokyo. Our collaborator, Shida, ruined his health during the unfavourable time of the war and had to leave from our work; but we fortunately received another young physicist Sakayanagi as a menber of our group.

Because the variation of the economic state after the War made the existence of the Institute impossible, it was replaced by the Scientific Research Institute, Ltd. established in 1947. Though the financial state is still not sufficient for the work on the grating, this work is now continued as a joint work by the Scientific Research Institute and the Institute of Optical Research attached to the Tokyo University of Education.

As we have written above, our machine was originally constructed about 25 years ago without any specially precise device. Accordingly it can not be compared with recent technics developed in the United States. Our efforts have been spent mainly on the correction of errors in the screw, and we see now a faint light on the future of our work of making gratings capable of use in research work. In the following we shall describe the present state of the work.

We must mention here that for several years our work has been finantially supported by the Ministry of Education. Also we are very thankful to the Mainich News Press Ltd. for giving us the Encouragement Gift of 1950 to further our work.

2 Structure of the Machine

The structure of our ruling engine is shown schematically in Fig. 1.

The main screw (1) has a pitch of 1 mm; it is 5 cm in diameter and 50 cm in length. A worm-gear (3) attached to the head of the main screw has 360 teeth, and the worm (4) can be rotated n/16 of a whole revolution by a ratch (6), so that it is possible to rule lines at a distance of $\frac{1}{360} \times \frac{n}{16}$ (n=1, 2.……16) mm. Another screw (21) which has a worm wheel (18) can move with the same speed as the main screw. This screw is coupled to the main screw with the aid of a gear (5) and of a worm (19) and this carries a cylindrical cam (20) which serves for the correction of the main screw. When an arm (23), touching to the cam, rotates slightly according to the surface form of the latter, it displaces the worm rod (4) back and forth by the movement of the contact point (24), and thus the rotation of the main gear (3) is modified from the mean revolution. The amount of the correction is measured by a needle attached to the arm of the cam, and the 0.6 mm of the needle corresponds to the 1/20 λ (Hg green line) of the grating movement. There is another correction device (17) on which an

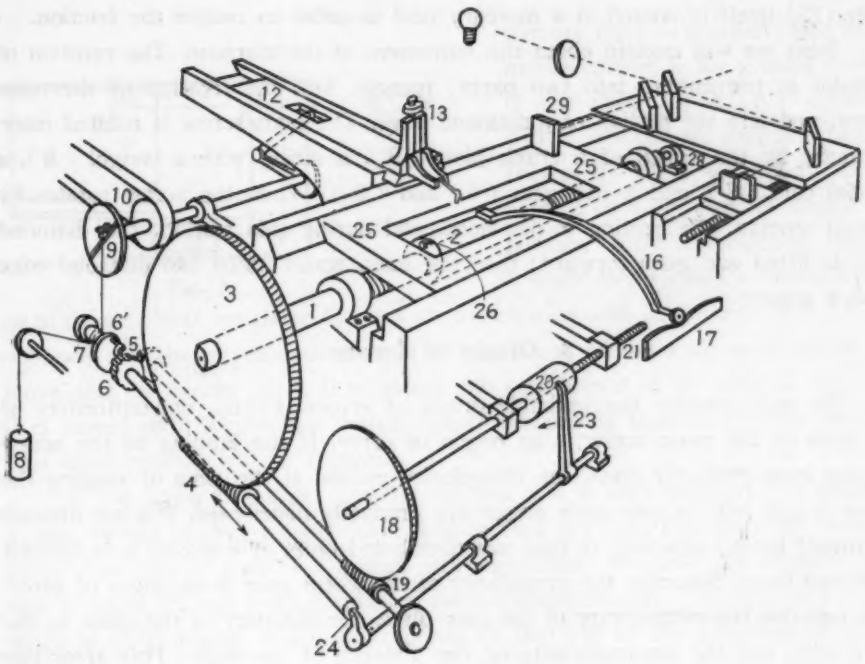

Fig. 1

arm (16) from the nut (2) is contacted. By the precise motion of this arm, the nut (2) is rotated back and forth, the result being the correction of the movement for a long range. 2/100 mm of the correction plate (17) corresponds to 1/20 λ of the screw. The end of the main screw is covered by a ruby plane, which contacts a steel ball at (28).

The grating to be ruled is placed on a heavy plate (25), which is pushed to move at the widia plane by a ball (26) attached to the nut (Fig. 2.) The

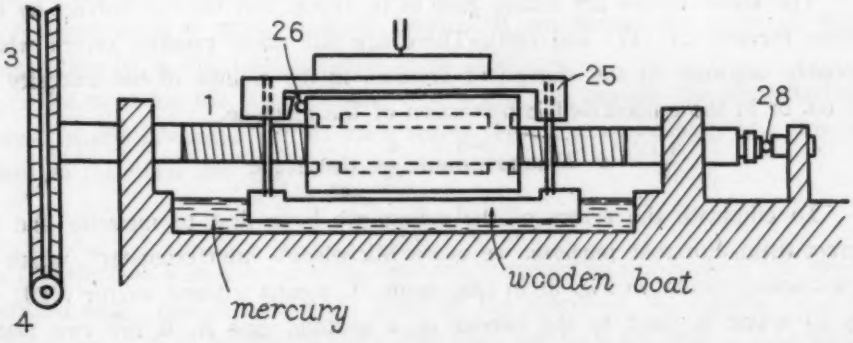

Fig. 2.

plate (25) itself is floated in a mercury pool in order to reduce the friction.

Next we will explain about the movement of the machine. The rotation of a motor is transmitted into two parts; namely, into the rotation of the main screw, and into the motion of a diamond edge. The main screw is rotated intermittently by the action of a crank plate (9), a string with a weight (8), a special cam (7), and a nail gear (6) and (6′). When the screw rotates by certain amount, the grating is displaced, and during this motion, the diamond edge is lifted and goes forward; then the main screw stops and diamond edge rules a groove.

3 Origin of Errors

We will consider the probable origin of errors. Firstly, non-uniformity of the pitch of the main screw is an origin of error. If the lapping of the screw has not been perfectly done, the irregularity caused at the time of making the screw is still left. In case such errors are gradually distributed, it is not difficult to correct them; however, if they are distributed quite at random, it is difficult to correct them. Secondly, the irregularity of the worm gear is an origin of error. This includes the excentricity of the gear plate, the obliquity of the plate to the screw axis, and the non-uniformity of the distance of the teeth. This error has a period of one revolution or some fraction of revolution, which depends upon the previous method of the construction of the gear. Thirdly, the in-coincidence of the axis of the screw and that of rotation is another origin of error. This circumstance means that the screw is oblique to the direction of the travel of the nut, and thus the nut does not move uniformly, but with a periodic small back and forth motion. To avoid this error, we adjust the inclination of the plate contacting the ball (26). The fourth origin of error is the thrust bearing of the main screw. If the ruby plane is not well polished and if the ball is not at the center of the rotation, the screw makes a back and forth motion.

The above errors are rather easy to be found, and we can correct by the proper forming of (17) and (20). There are still other random errors which probably originate in the change of friction, in the change of the viscosity of the oil, or in the unidentified imperfection of the machine.

4 Measurement of the error

To eliminate the errors of the ruling, we have first to measure and to correct them. For that purpose, we use a Michelson's interferometer[1], which is shown schematically in Fig. 3. In that figure, C means a plane mirror ((29) of Fig. 1) which is fixed to the carrier of a grating, and A, B are two plane

1) A. A. Michelson, J. of Franklin Inst., **181** (1916) 785.

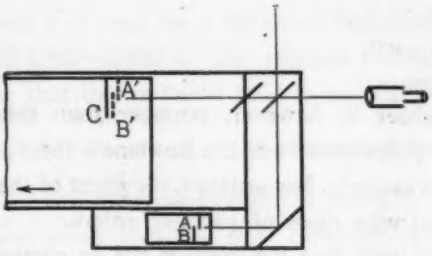

Fig. 3.

mirrors fixed to another plate which moves parallel to the grating carrier. If the image of A (A′) coincides with C, one can see nice interference fringes by using white light. In this case it is very easy to decide the position of the coincidence, because a slight in-coincidence causes a change of colour. Next we move C, until its coincidence with the image of B (B′) is obtained, and the corresponding angle of rotation a_1 of the worm gear is read. We move next the carrier of A, B to obtain the coincidence of A′ with C, and then C is moved until it coincides with B′, the corresponding angle of rotation being a_2. The same process will be repeated.

If the screw is perfect and the rotation of it is very uniform, the angle a_1, a_2, etc., should be always coincident; actually they are not. Therefore we form the cylindrical cam to make a_1, a_2, and etc., coincident. We took the distance of A and B about 1/9 mm and interpolated the intermediate part. The accuracy of the angle is 1/100 degree which corresponds to the 1/10 of the interference fringe. The error due to the excentricity of the worm gear plate, or that may be due to the incompleteness of the plate-and-ball contact, may have the period of one revolution. Such errors can be corrected by interpolation between 9 points in a revolution. However, if the teeth distance is so irregular that the accompanying errors have small periods within a revolution, nine points are not sufficient to observe them. In our instrument, this seems to be just the case, and observetions at smaller distance are desirable. In this case we have to observe so many points that the accuracy of measurements must be well considered.

Our problem is just the same as in the case of measuring a long distance with a very short scale. Suppose we measure 1 mm by successive measurements of n times using a small scale of $1/n$ mm. If we denote the error of single observation by Δ, the total probable error is $\sqrt{n}\,\Delta$

We consider the Rowland ghost of a grating, namely the error having a period of one revolution of the main screw. The relative intensity of a Rowland ghost to the main line is given by[2];

$$Ig=\frac{M^2}{4}\left(\frac{2\pi b}{a}\right)^2$$

In this formula a means a grating constant, b means an amplitude of the sinuous periodic error, and M means the order of the spectrum. We assume $b=\sqrt{n}\,\Delta$. The value of Δ is roughly $0.5/20\,\mu$ and thus for $n=9$ we have $\sqrt{n}\,\Delta=0.075\,\mu$.

2) H. A. Rowland, Phil. Mag., **35** (1893) 397.

Putting in $a=1.8\,\mu$, we get for $M=1$

$$Ig=\frac{4.3}{1000}$$

The observed intensity of the Rowland ghost is, however, stronger than this value, and the intensity distribution is fairly deviated from the Rowland's theory, and many ghosts of higher orders appear irregularly. For instance, the ghost of the 8th order is often very strong as compared with those of younger orders.

From those circumstances we can conclude that the error is not so simple as of the period of one revolution and there must be errors of still smaller periods. We have, therefore, to observe at more points than nine. In order to increase the accuracy, we used monochromatic light instead of white light. If we fix A and count the number of fringes, we can avoid the additive errors; but it is, of course, not easy to count some 4000 fringes per mm. However as we have already corrected under a fraction of the wave length using white light, we can fix a within the accuracy of one fringe. As we can read the fraction of a fringe accurately, we can determine the error of one revolution of the screw with the accuracy of Δ.

We used a mercury green line. Fig. 4, shows an example of the measurement. This shows a much more complicated curve than that of a period of one

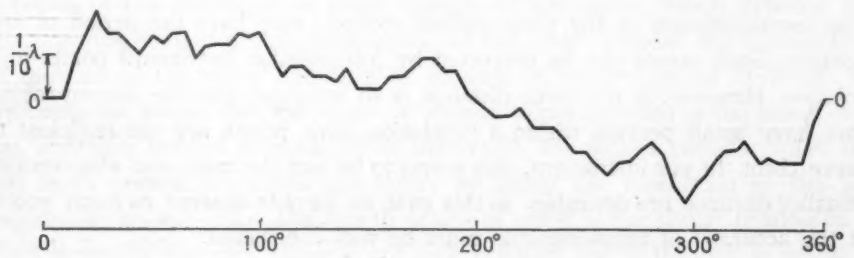

Fig. 4.

revolution. Repeating such observations, we get the total corrections for one revolution of the order of $1/2\,\lambda$ to $4\,\lambda$. The error of the long run is also corrected, first using white light, and then using monochromatic light. In this case we used a cadmiun red line instead of mercury green line.

5 Control of temperature

It is generally accepted that the constancy of the temperature under 1/100°C is required for the ruling of grating in order to avoid expansion of the machine and change in the viscosity of the oil. Our ruling machine is set in a small room located in a very big room. The big room has thick walls and no window, and the temperature variation in the room is about ± 1 C° in a day. The temperature in the small room is controlled with electric lamps and mercury-toluol controller,

and it is read by a Beckman thermometer. It is kept constant within the error of 1/100~2/100° C. The machine itself is covered by a double-walled wooden cover, so that the variation in it is supposed to be within 1/100° C.

6 Results obtained up to now

As mentioned in the introduction, we have made endeavour already more than five years since the war. Although our progress has been rather slow, we have nevertheless been successful in ruling gratings which can be used practically. The breadth of the ruled area is within 10 cm, and the length of the lines is about 4 cm. The number of lines is from 5,000 to 12,000 per cm. We are using speculum metal (Cu 68 %, Sn 32 %) which we cast ourselves. We rule on plane and also on concave surface, but the radius of curvature is shorter than 1.5 m.

The resolving power can not yet be satisfactory. For instance, the resolving power of a grating is 15,000 in the first order, where it is expected theoretically to be 30,000. A sample spectrum photographed by our grating (test No. 96) is shown in Fig. 5. The upper half of it is the spectrum of iron arc (exporsure 2 sec.), and the lower half is the overexposed (2 hours) 5461 line of Hg to exaggarate the character of Rowland ghosts of our grating. This No. 96 is one of the gratings which have most strong characteristic of ghost. One can see that the ghosts of the 2nd ond the 8th orders are fairly strong.

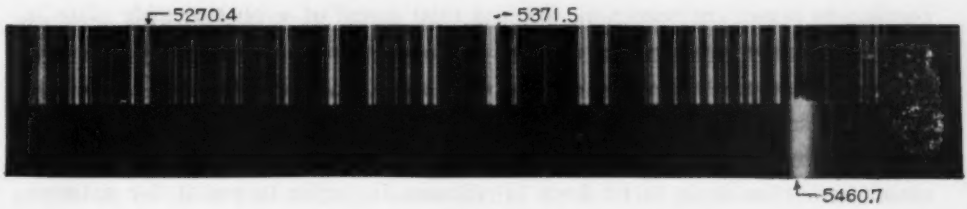

Fig. 5.

Recently many new technics for the ruling work of grating have been developed in America[3]. Diamond edges are polished to give proper form in America although we in Japan are still looking for an edge made by cracks. Aluminum coated glass surface is used in America instead of speculum metal; we are now preparing for this technics.

Nevertheless, we must consider that our machine was made more than 25 years ago. We are very desirous to construct a new machine according to more recent knowledge; however, at present the economical condition in Japan does not allow us to proceed.

3) G. R. Harison and J. E. Archer, J. O. S. A,. **41** (1951) 495: J. Strong, J. O. S. A., **41** (1951) 3; H. B. Babcoc and H. W. Babcac, J. O. S. A. **41** (1951) 776.

A New Mounting of Concave Grating Suitable for a Spectrometer

Masao SEYA

Institute for Optical Research, Tokyo University of Education

(Received November 14, 1951)

Recently the measuring technics of a spectrum by a photoelectric tube have made great development and various types of spectrometers have been invented to detect a spectrum by a photoelectric tube. The author have attempted to observe a spectrum by a photoelectric tube in a simplified mechanism namely fixing an entrance slit and an exit slit to observe a spectrum by a rotation of a grating.

1 Introduction

Since an ingenious invention by Rowland, the concave grating has become one of the most powerful weapons of spectroscopy and the method of using it has been developed in several ways. The fundamental principle is based on the character of the Rowland circle, and many well known methods such as the Rowland mounting, the Littrow mounting, the Paschen mounting, the Wadsworth mounting and so on have been brought into practical use. In each case, a photographic plate is usually used for detecting the spectrum.

Resently, the measuring technics of light by a photoelectric tube have become possible to detect the spectrum. When a tube insted of a photographic plate is used for concave grating spectroscopy, it is usually fixed after an exit slit on a Rowland circle and either the grating or the exit slit with the tube are moved along the circle, so that the light can reach the same place on the photoelectric surface. The mechanism of the spectrometer accordingly becomes rathar complicated, and when it is to be kept in vacuum in order to use it for extreme ultraviolet light, the vacuum vessel becomes inevitably large.

In spite of such inconvenience, several types of spectrometer with the photoelectric tube have been designed. In the first type a grating is displaced alonge a Rowland circle, and in the second type a grating is mounted in a Wadsworth mounting.

The first type was adopted by Fujioka and Ito[1] and the Baird Associates[2]. In these cases, an entrance slit and an exit one are fixed on a Rowland circle, and a grating is driven along the circle. For that purpose a grating holder is attached to an arm, which rotates about the center of the circle. To contain this mechanism, it is necessary to use a considerably large vacuum vessel. As another

1) Y. Fujioka and R. Ito, Science of Light (*Reports of Institute for Optical Research*) **1** (1951) 1;
2) Name of product, *Ultraviolet Spectrometer*.

defect of this mechanism, the part of the grating surface hit by the light beam varies according to the movement of the grating; therefore it is impossible to use the whole area of the ruled surface, causing the diminution of the resolving power.

The second, the Wadsworth mounting type was adopted by Kock, Taylor and Johnston[3]. The commendable characteristics of this type are the wide range of the measurable region, i. e. from 2000 Å to 14000 Å, and the linearity of dispersion. On the other hand, the weak point lies chiefly in the use of a reflecting mirror to change the incident light into a parallel ray. As the reflectivity of light by metals in the ultraviolet region is generally very small, the use of a mirror causes a great loss of intensity.

In the present paper the author has tried to search for a new type of mounting of a concave grating suitabie for a photoelectric tube spectrometer. The characteristics of this type should be as follows; an entrance slit and an exit one are fixed and only by the revolution of a grating should various parts of the wave length be obtained in good focus. To satisfy this condition, the two slits and the grating can not lie on a Rowland circle. We can show, however, the possibility of fulfilling this condition for wave length range of, for example 2500 Å—5000 Å. The applicable area of the grating surface can not be so large as the usual method based on the character of the Rowland circle, and this limitation of the surface area naturally diminishes the resolving power of the spectrum. Still, this type of mounting can afford a basis for construction of a simplified vacuum grating spectrometer.

In the following § 2, we present a brief summary of Beutler's theory of concave grating which gives the basis of further discussion. In § 3, we develop the theory and obtain a formula satisfying the above-mentioned condition. As it is difficult to solve the equation analytically, we use the graphical method and determine the proper relation of the two slits and a grating for the wave length of 5000 Å to 2000 Å, Although an actual spectrometer has not yet been constructed, we verified the calculated condition by means of the photographic method. In § 4, we give the experimental result.

2 Beutler's Theory on Concave Grating[4]

The Theory of a concave diffraction grating has been studied by many authors; among them, Beutler's treatment is quite thorogh and suitable for further application. According to Beutler, the condition for image formation can be treated as follows:

3) G. K. Kock, W. J. Taylor and H. L. Johnston: Jour. Opt. Soc. Amer., **41** (1951) 125;
4) H. G. Beutler, Jour. Opt. Soc. Amer., **35** (1945) 311.

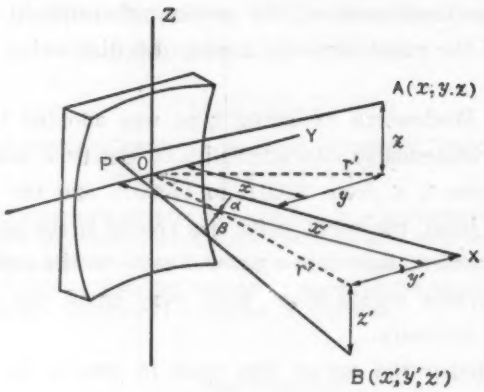

Fig. 1.

Set the origin of a cartesian coordinate O at the center of the grating surface, coincide the x-axis with the grating normal and make the x-axis parallel with the grooves of the grating. Let A (xyz), B (x'y'z'), P (ξ,w,l) be respectively the coordinates of the entrance slit, of the image, and of any point on the grating surface. Further let m be the order of a spectrum, λ the wave length, d the grating constant, R the radius of curvature of the grating, and r and r' the distances from the origin to the projective points of A and B on the xy plane, respectively (Fig. 1).

Now the light path function F is expressed by

$$F=AP+BP+(w/d)m\lambda. \tag{1}$$

m being an integer. The diffracted rays at various parts of the grating must reach to B in the same phase in order that they may reinforce each other. Accordingly, F must be kept constant within the limits of a quarter wave length, independently of the position of P. Denote the incident angle and diffracted angle by α and β respectively (the signs are opposite when A and B lie on different sides of the grating normal); then AP and BP are expressed as follows:

$$AP=F_1+F_2+F_3+F_4+F_5+F_6+F_7+\cdots\cdots,$$
$$BP=F_1'+F_2'+F_3'+F_4'+F_5'+F_6'+F_7'+\cdots\cdots,$$

where

$$F_1=r-w\sin\alpha$$
$$F_2=\frac{1}{2}w^2\left(\frac{\cos^2\alpha}{r}-\frac{\cos\alpha}{R}\right)+\frac{1}{2}w^3\frac{\sin\alpha}{r}\left(\frac{\cos^2\alpha}{r}-\frac{\cos\alpha}{R}\right)+\frac{1}{2}w^4\frac{\sin^2\alpha}{r^2}\left(\frac{\cos^2\alpha}{\gamma}-\frac{\cos\alpha}{R}\right)+\cdots\cdots,$$
$$F_3=\frac{1}{2}l^2\left(\frac{1}{r}-\frac{\cos\alpha}{R}\right)-\frac{lz}{r}+\frac{z^2}{2r},$$

$$F_4=\frac{1}{2}l^2w\frac{\sin\alpha}{r}\left(\frac{1}{r}-\frac{\cos\alpha}{R}\right)+\frac{w\sin\alpha}{2r^2}(-2lz+z^2),$$

$$F_5=\frac{(w^2+l^2)^2}{8R^3}\left(\frac{1}{r}-\frac{\cos\alpha}{R}\right),$$

$$F_6=\frac{-w^4}{8r^3}\left(\frac{\cos^2\alpha}{r}-\frac{\cos\alpha}{R}\right)^2-\frac{3w^3\sin\alpha}{8r^3}\left(\frac{\cos^2\alpha}{r}-\frac{\cos\alpha}{R}\right)^2,$$

$$F_7=\frac{(w^2+l^2)^2}{8R^3}\frac{w\sin\alpha}{\gamma}\left(\frac{1}{\gamma}-\frac{\cos\alpha}{R}\right),$$

$$F_1'=r-w\sin\beta,$$

$$F_2'=\frac{1}{2}w^2\left(\frac{\cos^2\beta}{r'}-\frac{\cos\beta}{R}\right)+\frac{1}{2}w^3\frac{\sin\beta}{r'}\left(\frac{\cos^2\beta}{r'}-\frac{\cos\beta}{R}\right)+\frac{1}{2}w^4\frac{\sin^2\beta}{r'^2}\left(\frac{\cos^2\beta}{r'}-\frac{\cos\beta}{R}\right)+\cdots\cdots,$$

$$F_3'=\frac{1}{2}l^2\left(\frac{1}{r'}-\frac{\cos\beta}{R}\right)-\frac{lz'}{r'}+\frac{z'^2}{2r'},$$

$$F_4'=\frac{1}{2}l^2w\frac{\sin\beta}{r'}\left(\frac{1}{r'}-\frac{\cos\beta}{R}\right)+\frac{w\sin\beta}{2r'^2}(-2lz'+z'^2),$$

$$F_5'=\frac{(w^2+l^2)^2}{8R^3}\left(\frac{1}{r'}-\frac{\cos\beta}{R}\right),$$

$$F_6'=\frac{-w^4}{8r'^2}\left(\frac{\cos^2\beta}{r'}-\frac{\cos\beta}{R}\right)^2-\frac{3w^3\sin\beta}{8r'^3}\left(\frac{\cos^2\beta}{r'}-\frac{\cos\beta}{R}\right)^2,$$

$$F_7'=\frac{(w^2+l^2)^2}{8R^3}\frac{w\sin\beta}{r'}\left(\frac{1}{r'}-\frac{\cos\beta}{R}\right).$$

The constancy of the terms $\left(F_1+F_1'+\frac{w}{d}m\lambda\right)$ and (F_2+F_2') give the conditions for image formation. The additive terms (F_3+F_3') give the astigmatism, (F_4+F_4') the comatic aberration and the curvature of the spectral lines, (F_5+F_5') the spherical aberration, (F_6+F_6') and (F_7+F_7') give higher order aberrations.

To obtain the condition for image formation, Fermat's principle is applied to $\left(F_1+F_1'+\frac{w}{a}m\lambda\right)$ and (F_2+F_2').

Thus from

$$\partial\left(F_1+F_2+\frac{w}{a}m\lambda\right)\Big/\partial\omega=0$$

we obtain

$$d(\sin\alpha+\sin\beta)=m\lambda \tag{2}$$

and from

$$\partial(F_2+F_2')/\partial\omega=0$$

we obtain

$$w\left(\frac{\cos^2\alpha}{r}-\frac{\cos\alpha}{R}+\frac{\cos^2\beta}{r'}-\frac{\cos\beta}{R}\right)+\frac{3}{2}w^2\left[\frac{\sin\alpha}{r}\left(\frac{\cos^2\alpha}{r}-\frac{\cos\alpha}{R}\right)+\frac{\sin\beta}{r'}\left(\frac{\cos^2\beta}{r'}-\frac{\cos\beta}{R}\right)\right]=0 \tag{3}$$

Equation (2) is the well known relation among α, β and λ, although this

equation gives no information on the focal conditions for the concave grating, since r and r' are not involved in it.

3 Condition for the image formation at a definite point independent of the revolution of the grating

Equation (3) determines the position of the image when α, r and β are given. If the entrance slit and the exit slit lie on a Rowland circle,

$$\frac{\cos^2\alpha}{r}-\frac{\cos\alpha}{R}=\frac{\cos\alpha}{R}-\frac{\cos\alpha}{R}=0, \qquad \frac{\cos^2\beta}{r'}-\frac{\cos\beta}{R}=\frac{\cos\beta}{R}-\frac{\cos\beta}{R}=0,$$

which shows that the equation (3) is identically astisfied. In the case of Wadsworth mounting $r=\infty$, $\beta=0$ which also manifest that the equation (3) is identically satisfied. Only in these two cases can equation (3) be identically perfect. In all other cases (3) can not be satisfied; that means there is no mounting to give perfect focus except in the two cases. However, as the equation (3) can be considered as an expansion in the power of w/R, the second and the higher terms can be neglected approximately or can be considered as an aberration. Then equation (3) reduces to

$$\frac{\cos^2\alpha}{r}-\frac{\cos\alpha}{R}+\frac{\cos^2\beta}{r'}-\frac{\cos\beta}{R}=0 \tag{4}$$

If we give α, β, r and r' such values as to satisfy epuation (4), the set of (α, r) and (β, r') are the positions of the entrance slit and its image, namely the exit slit. If we denote the lefthand side of the equation (4) by f, then

$$f=\frac{\cos^2\alpha}{r}+\frac{\cos^2\beta}{r'}-(\cos\alpha+\cos\beta)/R \tag{5}$$

Our problem is now to look for a condition that $f=0$ and r, r' and $(\alpha-\beta)$ are independent of the value of α.

Put $\alpha-\beta=C$ or $\beta=\alpha-C$. Then equation (5) becomes

$$f=\frac{\cos^2\alpha}{r}+\frac{\cos^2(\alpha-C)}{r'}-\frac{\cos\alpha+\cos(\alpha-C)}{R}. \tag{6}$$

Before treating equation (6) we examine how the value of α has to vary in order to observe various parts of the spectrum. We give C several definite values such as 15°, 30°, 60°, 90°, 120° and calculate the value of α correspoding to 0Å, 1000Å, 2000Å, 4000Å, 5000Å using equation (2) (the grating constant being assumed 1500/inch). The results are listed in Table 1 and shown in Fig. 2. When the value of C exceeds 90°, the variation of α increases rapidly, but when it is smaller than 90°, the amount of variation of α does not exceed 11°45′. For instance, if we settle the value of C as equal to 90°, α changes from 45° to 56°45′ (or from 45° to 33°15′) corresponding to the spectrum range from 0Å to 5000Å. If the grating is set at the position $\alpha=45°+\frac{56°45'-45°}{2}$ $\left(\text{or } 45°-\frac{45°-33°15'}{2}\right)$,

Table 1

λ \ C	15°		30°		60°		70°		90°		120°	
1000 Å	9°10′	5°50′	16°42′	13°18′	31°54′	28° 6′	37° 1′	32°59′	47°20′	42°46′	63°18′	56°42′
2000 Å	10°50′	4°10′	18°25′	11°35′	33°49′	26°11′	39° 2′	30°58′	49°40′	40°20′	66°37′	53°23′
3000 Å	12°30′	2°30′	20° 8′	9°52′	35°44′	24°16′	41° 3′	28°57′	52° 1′	37°59′	69°57′	50° 3′
4000 Å	14°11′	49′	21°51′	8° 9′	37°39′	22°21′	43° 5′	26°55′	54°23′	35°37′	73°19′	46°41′
5000 Å	15°51′	−51′	23°35′	6°25′	39°35′	20°25′	45° 8′	24°52′	56°45′	33°15′	76°45′	43°15′
6000 Å	17°32′	−2°32′	25°19′	4°41′	41°31′	18°29′	47°11′	22°49′	59° 9′	30°51′	80°13′	39°47′
$\Delta\alpha$	8°22′		8°37′		9°37′		10°10′		11°49′		16°55′	

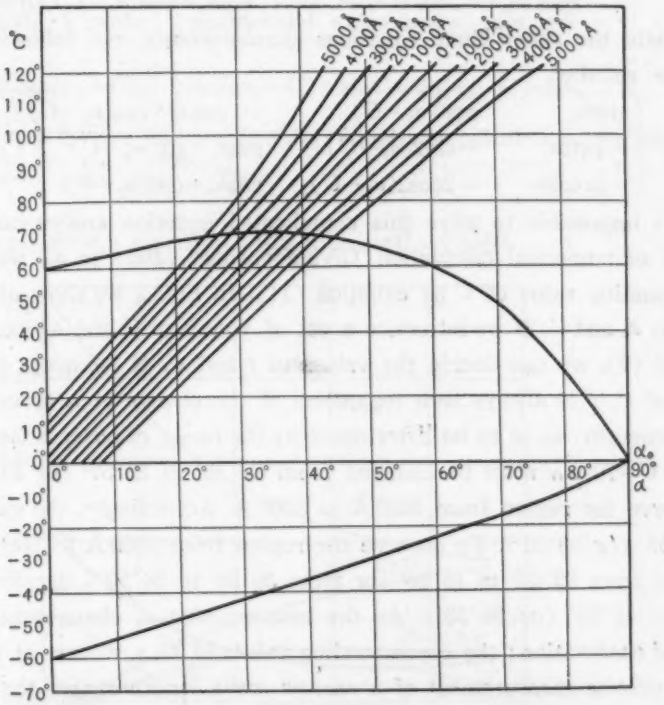

Fig. 2.

it must be rotated within the angle ±5°53′. The rotation angle of the grating is ever smaller than 5°53′ when the value of C is less than 90°. In Fig. 2 we can see the relation between C, a and λ.

As the variation of a is small, we may put in $a=a_0+\Delta a$ and expand the equation (6) according to Taylor's formula. Then

$$f=\cos^2(a_0+\Delta a)/r+\cos^2(a_0+\Delta a-C)/r'-[\cos(a_0+\Delta a)+\cos(a_0+\Delta a-C)]/R$$
$$=\cos^2 a_0/r+\cos^2(a_0-C)/r'-[\cos a_0+\cos(a_0-C)]/R$$

$$+\left\{-\sin 2a_0/r-\sin 2(a_0-C)/r'+[\sin a_0+\sin(a_0-C)]\frac{1}{R}\right\}\frac{\Delta a}{1}$$

$$+\left\{-2\cos 2a_0/r-2\cos 2(a_0-C)/r'+[\cos a_0+\cos(a_0-C)]\frac{1}{R}\right\}\frac{\Delta a^2}{2}$$

$$+ \qquad (7)$$

We neglected higher terms because Δa is a smal quantity, the order of magnitude of 4th term is smaller than the 2nd term of equation (3) which is neglected in calculation. The condition that f becomes zero regardless of the value of Δa is now

$$\cos^2 a_0/r+\cos^2(a_0-C)/r'-[\cos a_0+\cos(a_0-C)]/R=0 \qquad (8)$$

$$-\sin 2a_0/r-\sin 2(a_0-C)/r'+[\sin a_0+\sin(a_0-C)]/R=0 \qquad (9)$$

$$-2\cos 2a_0/r-2\cos 2(a_0-C)/r'+[\cos a_0+\cos(a_0-C)]/R=0 \qquad (10)$$

To satisfy the above three equations simultaneously, the following determinant must be satisfied.

$$\begin{vmatrix} \cos^2 a_0 & \cos^2(a_0-C) & -[\cos a_0+\cos(a_0-C)] \\ -\sin 2a_0 & -\sin 2(a_0-C) & \sin a_0+\sin(a_0-C) \\ -2\cos 2a_0 & -2\cos 2(a_0-C) & \cos a_0+\cos(a_0-C) \end{vmatrix}=0 \qquad (11)$$

As it is impossible to solve this complicated equation analyitically, we adopt a method of numerical calculation. Giving various values to a_0, we calculated the corresponding value of C by equation (11). In Fig. 2 we show also this relation between a_0 and C. If we introduce a set of values of C and a_0 into the equations (8) and (9), we can decide the values of r and r'. If we adopt these values a_0, C, r and r', f is always zero regardless of the change of α around α_0.

Generally, α_0 is to be determined by the range of observation. For instance, setting $C=70°$, α must be changed from 32°59′ to 28°57′ (or 37°01′ to 41°03′) to observe the region from 1000 Å to 3000 Å. Accordingly, the value of α_0 must be 30°58′ (or 39°02′). To observe the region from 2000 Å to 5000 Å, α must be changed from 39°02′ to 45°08′ (or from 30°58′ to 24°52′), deciding the value of α_0 to be 42°05′ (or 36°55′). As the proper value α_0 changes according to the range of observation; the corresponding values of C, r, r' vary at the same time, In the precise measurement of a narrow wave length range, the suitable value of α_0 must be different for each range.

In the design of a spectrometer, the variation of C causes a rather complicated mechanism. If we can find some proper value of C which is independent of the change of α_0, it will be the most suitable value for the design of a spectrometer.

In the graph of α_0 and C shown in Fig. 2 there are three branches. Among these branches if we could dlscover such a branches as to satisfy $\partial C/\partial\alpha_0=0$ for some wide wave length range, we could adopt this value of C for this range.

The lowert branch is useless, because there is no part which satisfies the condition $\partial C/\partial\alpha_0=0$ and because the measurable range of this branch contains neither an extreme ultraviolet nor a visible region. The middle linear branch satisfies the condition perfectly, but we can not use this branch because it is necessary to set the entrance slit, the exit slit, and the grating on a straight line. The uppermost branch has a maximum point at $\alpha=35°$ and $C=70°$, and around this point it satisfies $\partial C/\partial\alpha_0=0$. This part looks to satisfy the required condition, but we have further to investigate the variation of r and r' caused by the rotation of the grating. For that purpose we give several values of C around $C=70°$, and observe how the value of r and r' varies in each case. From equation (8) and (9) r and r' are solved as follows:

$$r=2\cos(\alpha_0-C)\sin C\Big/\left\{\frac{1}{2}\sin 2\alpha_0+\sin C+\sin\alpha_0\cos(\alpha_0-C)\right\}\times R \tag{12}$$

$$r'=2\cos C\sin(\alpha_0-C)\Big/\left\{\frac{1}{2}\sin 2(\alpha_0-C)+\sin C+\sin(\alpha_0-C)\cos\alpha_0\right\}\times R \tag{13}$$

As these equatins are inconvenient for numerical calculation, we introduce new variables $\rho=\frac{R}{r}$ and $\rho'=\frac{R}{r'}$. Then

$$\rho=\frac{1}{4}\sin 2\alpha_0\sec(\alpha_0-C)\operatorname{cosec}C+\frac{1}{2}\sin\alpha_0\operatorname{cosec}C+\frac{1}{2}\sec(\alpha_0-c) \tag{14}$$

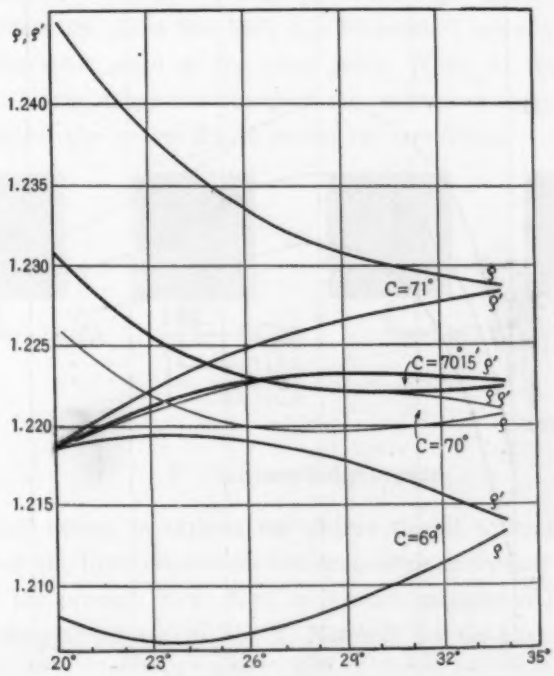

Fig. 3.

$$\rho'=\frac{1}{4}\sin 2(\alpha_0-C)\sec\alpha_0\operatorname{cosec}C+\frac{1}{2}\sin(\alpha_0-C)\operatorname{cosec}C+\frac{1}{2}\sec\alpha_0 \qquad (15)$$

If ρ and ρ' are constant independently of the change of α_0 for some definite value of C, this set of values of C, ρ, ρ' will be the most suitable one for the design. Putting various values to C at and around 70° in equation (14) and (15), the values ρ and ρ' against α_0 are calculated and shown in Fig. 3. Actually, the following 5 values 71°, 70°15′, 70°10′ 70°, 69° are given to C. The change of ρ, ρ' in the region 500 Å—3500 Å (α: 28°~34°) is minimum when C=70°15′ and the differences between the greatest and the smallest values of ρ and ρ' do not exceed 3×10^{-4}. This means that, if we use a 1 m concave grating, the changes of r and r' do not exceed 0.1 mm. If we want to observe a wider region, a somewhat smaller value of C, such as 70°10′, 70°, will be suitable, as is shown in Fig. 3.

We adopt 70°15′ as the value of C. The next problem is to decide the most suitable values of ρ and ρ' as they still vary slightly. From equation (12) the minimum value of ρ is 1·22220. We have to examine the change of ρ' when we adopt some definite values at and around 1.22220. We select 3 values ρ (1) 1.22220 (2) 1.22233 (3) 1.22247 and put in the following equation (16) and exa-

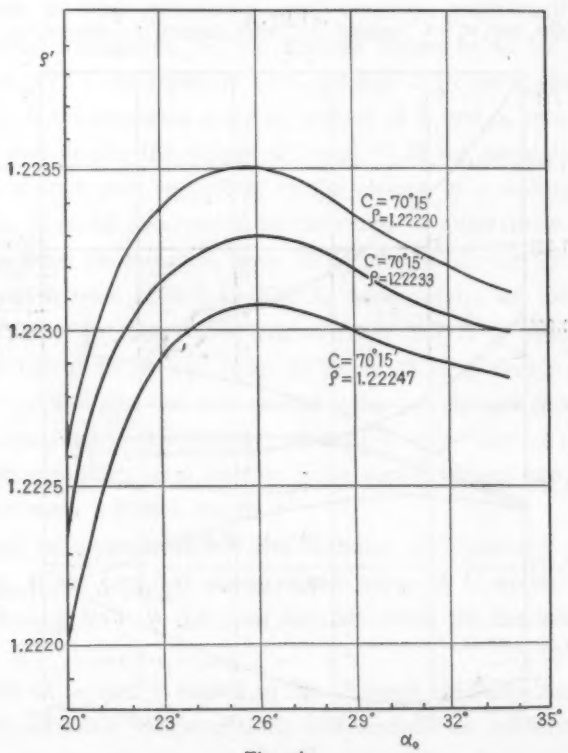

Fig. 4.

mine the variation of ρ' with α.

$$\rho'=\cos\alpha\cdot(1-\rho\cos\alpha)\sec^2(\alpha-C)+\sec(\alpha-C) \qquad (16)$$

The result is shown in Fig. 4. As the value of ρ grows greater than 1.22220, the change of ρ' near the maximum grows flatter, but the curves remove toward the right as a whole. The left hand side of each curve shows a great variation of ρ', and we can not use these regions. If we want to observe only the ultraviolet region, the value of ρ a little greater than 1.22247 will be suitable, and to observe a wide range, a little smaller value than 1.22247 will be better. If we adopt as the value of ρ 1.22247, the change of ρ' with α is smaller than 0.00023; namely, the change of r' is smaller than 0.15 mm when we use a 1 m concave grating whithin the range $35°=\alpha=21°30'$ the corresponding wave leng is 6600 Å−0 Å.

4 Proof of the result by the photographic method

We are now constructing a new vacuum spectrometer according to the principle of the preceding disscusion. Besides, to verify the theoretical data more briefly, we used the photographic method. We chose a concave grating of a 3 meter radius, of 15000 line per inch, and mounted in the following condition:

C 70°15′ $\rho=1.22247$

As the light source, we used a Hg lamp. At first the exit slit was adjusted at the position where the green line 5461 Å is focussed. Then removing the slit, we placed a photographic plate at the same place. When we rotate the grating, a different wave length image is focussed at the position of the exis slit, and every time photographed the image. Fig. 5 shows the spectrum.

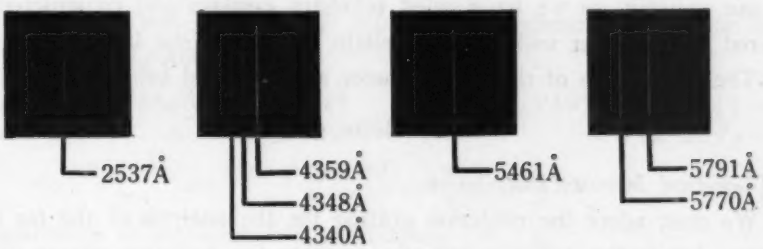

Fig. 5.

5 Acknowledgements

The writer wishes to express his sincere thanks to Professor Yoshio Fujioka, director of the Institute, for his encouragement and much valuable advise in the course of the present work. Also, he is much indebted to Dr. Yoshio Tanaka for his kind suggestions and to Mr. T. Namioka for his kind help in calculation.

Construction of a Far Infra-Red Spectrometer with Echelette Grating.

Hiroshi YOSHINAGA and Yahiko YAMADA
Department of Applied Physics, Faculty of Engineering, Osaka University

(Received December 10, 1951)

In order to analyze the far infra-red radiation, the echelette gratings of grating constant 12.5–50 μ have been ruled and examined on the groove form and the diffracted intensity distribution on each order by the residual ray of quartz. About 60 % of radiation energy is concentrated in the first order at one side. A far infra-red spectrometer of the Michigan spectrometer type was constructed with these echelette gratings, and the test of this spectrometer was performed by the residual rays from some crystals and by the absorption of CS_2 and CCl_4 molecules. The results show that this spectrometer is useful to 35 μ or more and has the resolving power of 0.8 cm^{-1} at 25 μ.

1 Introduction

Recently there were many developments for the Infra-red spectroscopy, particularly for the instrumentation in this region. But most of these instruments have prisms of artificial alkali halide crystals, for example, NaCl, KBr and KI etc., as the despersive medium, but there are limiting transparent wave-lengths for these prisms.

For longer wave-length region than prism region, we have to take the "Echelette Grating". There is no maker of the grating and the spectrometer with it in our country, so we have ruled echelette grstings and constructed the far infra-red spectrometer with those echelette gratings in our laboratory.

The test results of this spectrometer are described below.

2 Echelette grating

1. *Theoretical Intensity Distribution*

We must adopt the reflection grating for the analysis of the far infra-red rediation, but in the ordinary reflection grating the radiation energy distributes on all orders of spectra, especially the zero order spectrum in the direction of the specular reflection is the strongest. Therefore, if we use the echelette grating, instead of the ordinary reflection grating in which we use the only dim spectrum, we can get the most energy on a desired order in one side, and the bright spectrum may be used for the analysis.

The echelette grating has the surface of triangle grooves shown in Fig. 1. What characterizes this above all things, is that the effective surface of the diffraction is not the grating surface but the slow slope of the groove.

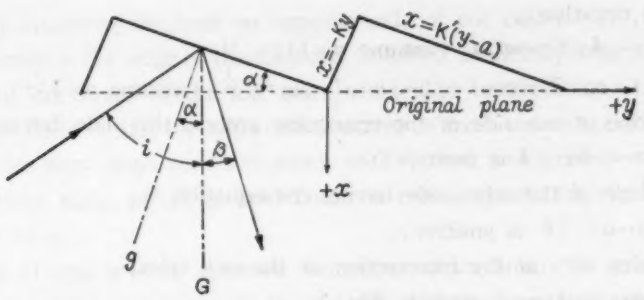

Fig. 1. Groove form and its coordinate system.
G, normal to the original plane.
g, normal to the slow slope of the groove.

In Fig. 1 we put i, incident angle; β, diffracted angle; d, grating constant; α, angle between the original plane of grating and the wall of a groove

$$m\lambda=d(\sin i\pm\sin\beta),$$
$$\alpha=(i\pm\beta)/2.$$

where m is the order and λ is the wave-length[1]. From these equations we can get the strongest radiation on one order and can determine λ if we know m, d, i, β and α. For upper signs throughout, the incident and diffracted rays are on the same side of the normal to the grating, while for lower signs they are on opposite side.

The dispersion and the resolving power are written as follows:

$$d\beta/d\lambda=m/(d\cos\beta), \qquad \lambda/d\lambda=mN.$$

where N is the total number of the grooves.

R. F. Stamm and J. J. Whalen[2] calculated the intensity distribution in each order, which is proportional to

$$n^2\left\{\frac{1+k^2}{(\mu-k\nu)^2}\sin^2\frac{\pi p(\mu-k\nu)}{\lambda}+\frac{1+k'^2}{(\mu+k'\nu)^2}\sin^2\frac{\pi(d-p)(\mu+k'\nu)}{\lambda}+\frac{[(1+k^2)(1+k'^2)]^{\frac{1}{2}}}{(\mu-k\nu)(\mu+k'\nu)}\right.$$
$$\left.\times\sin\frac{\pi p(\mu-k\nu)}{\lambda}\sin\frac{\pi(d-p)(p+k'\nu)}{\lambda}\cos\frac{\pi}{\lambda}[(\mu+k'\nu)(d-p)-p(\mu-k\nu)]\right\}.$$

The significance of the symbols is as follows:

d, the grating constant;

λ, the wave-length of the light;

m, the order of the spectrum (positive if on the same side of zero order as incident beam, otherwise negative);

n, the refractive index of air;

i, the angle of incidence (always positive);

β, the angle of diffraction (positive if on the same side of grating normal as

1) H. D. Babcock, J. O. S. A., **34** (1944) 1; 2) R. F. Stamm and J. J. Whalen, J. O. S. A., **36** (1946) 2.

i, otherwise negative);

$\mu=n(\sin i+\sin\beta)=m\lambda/d$ (assume $n=1$);

$\nu=n(\cos i+\cos\beta)=\cos i+[1-(m\lambda/d-\sin i)^2]^{\frac{1}{2}}$ (assume $n=1$);

k, the slope of one side of the triangular groove, this side having the equation $x=-ky$ (k is positive);

k', the slope of the other side having the equation

$x=k'(y-a)$ (k' is positive);

p, the value of y at the intersection of the two sides.

The coordinate system is clear in Fig. 1.

2. *Echelette Grating Material*

The echelette grating materials must have high reflectivity and properties suitable for easy ruling and polishing. Most of metals have good reflectivity for the far infra-red radiation.

As the material for the ordinary fine space grating is used the speculum metal alloyed with copper and tin, which is able to be polished as glass plate. But the speculum metal is not suitable for the echelette grating, because this grating must be cut deep comparably and the ruling cutter takes chattering at the alloy boundary where the metal changes its hardness. We adopted the copper plate considering the above conditions.

At first, we attempted to polish electrolytically the copper plate, but our desired area of the grating is too large to polish uniformly over whole surface, 17×18 cm by this method. Secondly, we deposited the copper layer on the flat glass plate by the vacuum evaporation method, but the layer comes off from the boundary surface often in ruling.

At last it was found to obtain good surfaces by polishing with chromium oxide as the abrasive and on the soft pitch disk mixed with paraffin of about 1/3 portion, as the rouge for glass polishing penetrates into the copper surface and makes it black and hard. The copper plates so polished are of the precision of five fringes tested by Newton's ring method.

3. *Ruling*

A comparator was modified to the ruling machine of "balancing load type". This machine has a principal screw of 1 mm pitch and of 2 cm diameter. Worm and worm gear which have 1/40 gear ratio are attached to the right end. Then the carriage advances in 1/40 mm by one revolution of the worm. The plane iron plate ($20\times19\times1$ cm) is fixed on the carriage to mount the grating material on it.

The holder of the ruling cutter reciprocates in the guide of "V" shape normal to the comparator screw. The ruling cutter is fitted at the top end of this holder, and is moved up and down by a cam. The depth and width of grooves

regulated by changing the load on opposite side of the cutter.

The cutter is the edge of the diamond polished artificially into pyramid, and the radius of curvature of the top point seemed to be about 2μ. To rule good grooves, it is desired that the edge of the cutter is fixed towards the direction of ruling and the slow slope comes in touch with a next new groove which will be ruled. We must make effort to hold constant ruling speed, for our apparatus is working by hand.

Errors of the grating constant occurring often from the principal screw errors of the ruling machine cause the "ghost" and scattered light. We found the periodical errors of our ruling machine screw of which period is 1 mm and the amplitude about $\pm 2\mu$. We examined the echelette grating ruled by this machine under the Zeiss universal measuring machine and made a compensation curve for these erorrs, but the errors are comparable with the limiting measurable value of the measuring machine and are not constant every ruling and every portion of the principal screw. Therefore, we used the direct reading method as follows.

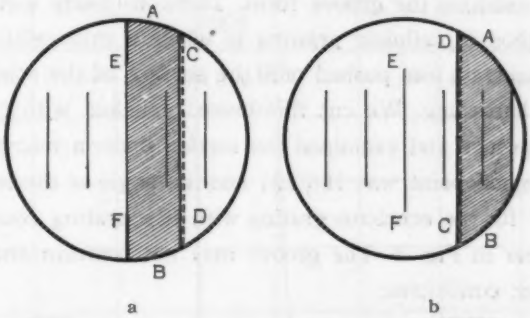

Fig. 2. Field of the microscope. Hatching part is the groove. Dotted line CD is the movable line.

The fixed micrometer microscope is adjusted to focus on the blade edge of the cutter on the grating material, and Fig. 2 shows the field of the microscope. EF and their adjacent short lines apart with equal distance are the scales of the eyepiece in the micrometer microscope and CD is a movable line. Now if the distance between CD and EF is equal to the desired grating constant, we take the first ruling, and the groove AB is ruled in Fig. 2 a. By the revolution of the worm of the ruling machine, the groove AB moves only by the grating constant as shown in Fig. 2 b, and we take the second ruling. Repeating this procedure the grating constants are determined by the distance between EF and CD, and the errors of the grating constant occur only on the superposition of the groove edge and the scale line in the eyepiece, and are less than 0.2μ.

So far as we take the above procedure, it is not necessary to use the interferometer method generally used in the fine space ruling.

Fig. 3. Groove form by celluloid printing.

4. Examination

It is the special feature that the echelette grating concentrates the energy into the first order spectrum of one side by controlling its groove form, and it is important to examine the groove form. There are many methods to do, so we adopted the method of celluloid printing in which a thin celluloid plate softened with the amyl accetate was pushed onto the surface of the echelette grating and taken off after hardening. We cut this casted celluloid with microtome perpendicularly to the groove and examined the section under a microscope. The ruling edge of the diamond point was 108°20′, and the angle of the intersection of two sides was 108°1′ for the echelette grating with 40 μ grating constant. The groove form is seen clear in Fig. 3. The groove may not conform always to the ruling point under other conditions.

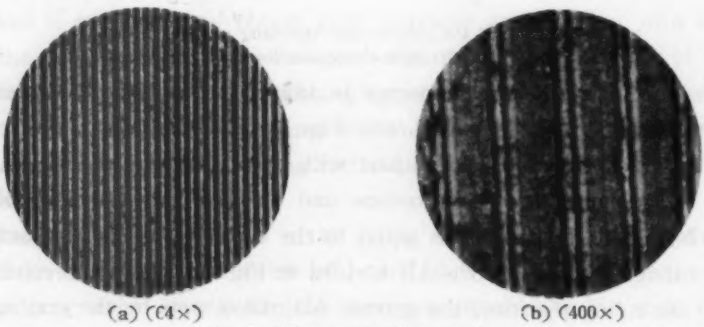

(a) (64×) (b) (400×)

Fig. 4. Microscopic photography.

Fig. 4 shows the microscopic photography of the echelette grating surface focused upon the top of the groove. Two thin parallel lines in Fig. 4 a (64×) show the tops of the grooves and it is shown that the unruled flat surfacers of the grating remained. Fig. 4 b shows the 400× microscopic photography of the same part of the grating described above also focused upon the tops of the grooves.

The faint line in the middle of grooves shows the bottom line.

In order to know the practical energy distribution on each order spectrum caused by those echelette gratings, we used the residual ray from crystalline quartz plates as the monochromatic light source to except the overlapping of the shorter wave-length radiation. The echelette grating is the most effective for the radiation of which wave-length is the same of the grating constant. But strong radiation is necessary to measure the energy distribution on higher order spectra of very weak energy. From these reasons, we used the strong residual ray of the crystalline quartz plate at the region of 8~9 μ, though this wave-length is shorter than the desired wave-length for our echelette grating. The spectrometer used for this examination is described in the next section.

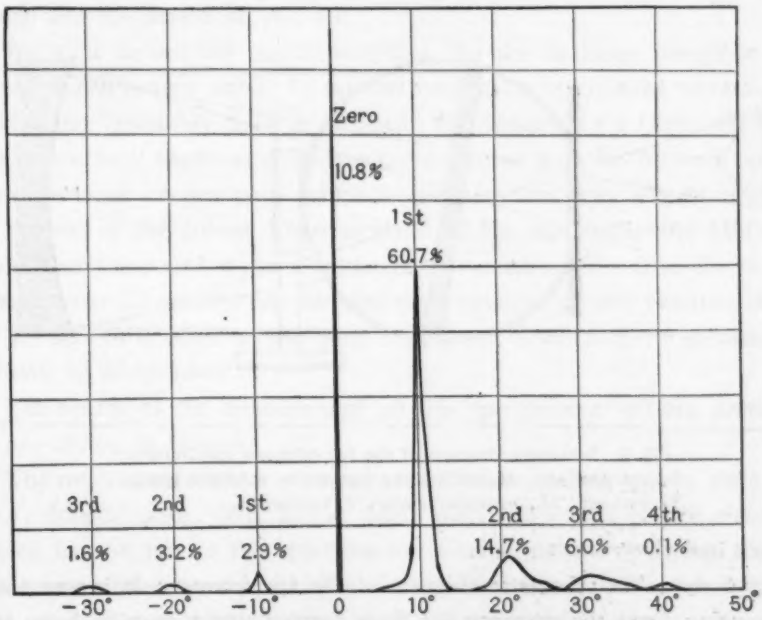

Fig. 5. Energy distribution in each order.

The echelette grating ruled on the copper plate, 10×12 cm ruling area, was silvered to increase the reflectivity instead of aluminium for easiness in vacuum evaporation. Fig. 5 shows an example of the distribution of these echelette gratings (grating constant 25 μ). Integrating these curves by a planimeter we get the results shown in Fig. 5 and Table 1.

TABLE. 1. Energy distribution on each order. (%)

Order	4	3	2	1	0	−1	−2	−3	−4
Cal.	0.03	2.48	0.68	79.66	0.04	7.84	2.85	3.16	3.08
Obs.	0.1	6.0	14.7	60.7	10.8	2.9	3.2	1.6	0.0

The intensity 10.8 % at the zero order may contain the radiation reflected from the very narrow surface remained unruled between grooves. The calculated values of distribution from the above Stamm's equation are also shown in Table 1 for the purpose of comparison with ours.

The far infra-red spectrometer with the echelette grating

H. M. Randall and F. A. Firestone[3] described an infra-red spectrometer of large aperture with suitable gratings. We constructed the far infra-red spectrometer with our echelette gratings described above and tested the characteristics of this spectrometer.

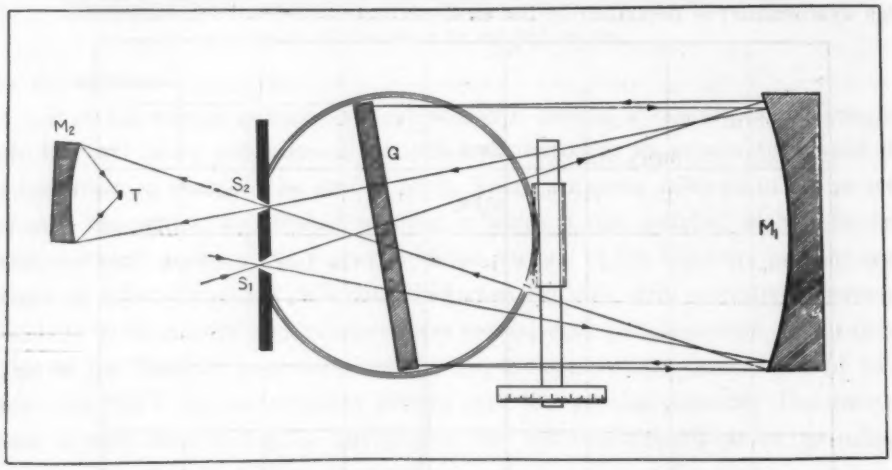

Fig. 6. Schematic diagram of the far infra-red spectrometer.
S_1, entrance slit; M_1, collimating mirror; G, echelette grating; S_2, exit slit; M_2, spherical mirror; T, thermopile.

1. *Design and Construction*

Fig. 6 shows the schematic diagram of the spectrometer. It is seen that the light diverging from the entrance slit S_1 is formed into a parallel beam by the paraboloidal mirror M_1 and directed against the grating G. Returning from the grating, the light again strikes the mirror M_1, and is then converged upon the exit slit S_2. An image of the exit slit reduced in linear dimension by about factor of 9 is focused upon the thermopile T by the spherical mirror M_2.

All optical parts, that is, the grating (17×18 cm in area), the collimating mirror (34 cm in diameter, 161 cm in focal length f and $\frac{\Delta f}{4f} < \frac{1}{10000}$ for each zone), and two bilateral slits (2 cm in length) are fastened to a single base consisting of a piece of 25 cm I-beam of 2 meter length. The grating table may be swung

3) H. M. Randall, R. S. I., 3 (1932) 196; H. M. Randall and F. A. Firestone, R. S. I., 9 (1938) 404; H. M. Randall, Rev. Mod. Phys., 10 (1938) 72.

into desired position by means of the worm and worm gear, of which the gear ratio is 1 : 240. The grating table is carried on a cone having a double taper. The angular position of the grating is determined with a graduated circle, and one division of the scale corresponds to 54″ rotation of the grating. This value corresponds to the wave-length shift 0.0110 μ at 25 μ, 0.0105 μ at 30 μ, 0.0145 μ at 35 μ for 25 μ grating. The entrance slit and the exit slit are adjusted in width by one operation, for this spectrometer is Littrow type. The detector is the thermopile consisted of two tellurium-constantan junctions, the sensitivity of 3.12 μV/μW, the internal resistance of 31.8 ohms, the receiver area of 1×1 mm. This thermopile is connected through the galvanometer which has the sensitivity of 7.45×10^{-10} A, 4.1×10^{-8} V, internal resistance of 25 ohms, critical damping resistance of 30 ohms and the period of 10.2 sec.

We want to use the optical amplifier, for the radiation energy in the far infra-red region is very small. To use this method the mechanical vibration of the ground of our laboratory must be reduced. We constructed a frame, $80 \times 80 \times 300$ cm, with the steel angle materials, the galvanometer is on the Müller's suspension put on the large wooden plate which is hung by four wire strings of 2 m long from the top of the frame. There is about 30 Kg load under the Müller's suspension, then the period of the vibration of galvanometer free from the thermopile increases from 1/2 sec to 4 sec, and also the amplitude of this vibration decreases from 1.5 mm to 0.3 mm on the lamp scale apart 3 m from the galvanometer.

2. *Results of Measurement*

The retults of the measurement by this spectrometer of 25 μ grating constant, are shown as follows:

The residual rays which were reported from crystalline quartz plate: 8～9 μ, 20.75 μ; fluorite plate: 23 μ, 32.8 μ; MgO plate: 15～19 μ; calcite plate: 29.4 μ, are used for the test of the spectrometer. Comparing the resolving power with prism spectrometer, we found in Fig. 7 the fine structure of the residual rays of quartz at 8～9 μ reported by Silverman[4]. The residual ray of the fluorite plate could be hardly seen through the wave-length from 20.5 to 24.5 μ, but in the region of 32～33 μ there was a peak at the wave-length of 32.8 μ, and the fine structure seemed to exist.

These measured curves of the residual rays are shown in Figs. 7～10, the radiation source being the globar.

We also measured the absorption of a few chemical compounds, CCl_4, and CS_2. The results of these measurements are shown in Figs. 11～12. In the measurements of CCl_4 and CS_2, the absorption cell, which was 3 cm long and fitted with 0.5 mm KBr plate windows, contained CCl_4 and CS_2 vapor saturated at room

4) S. Silverman and J. D. Hardy, Phys. Rev., 37 (1931) 176.

temperature (24° C), and the slit width of the spectrometer was 0.9 mm.

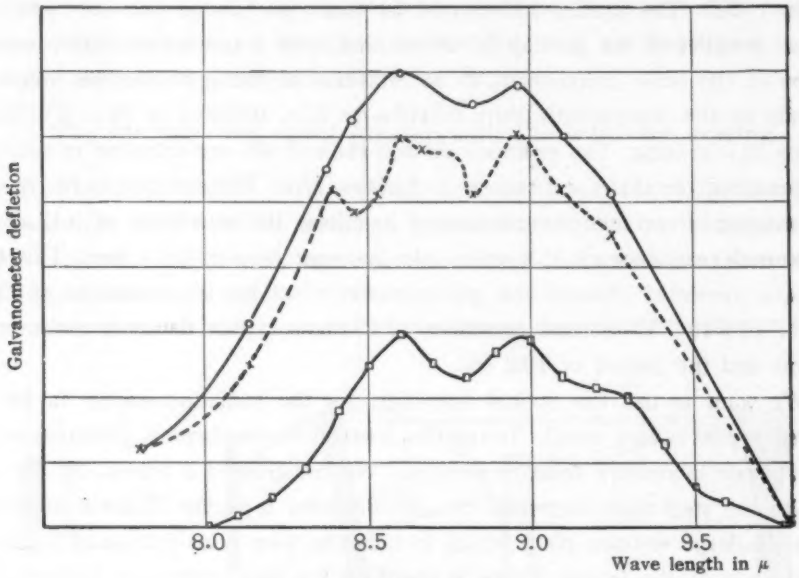

Fig. 7. Quartz residual ray.
○—○—○ Echelette grating, slit width 2 mm:
×----×----× Echelette grating, slit width 1 mm;
□—□—□ KCl prism.

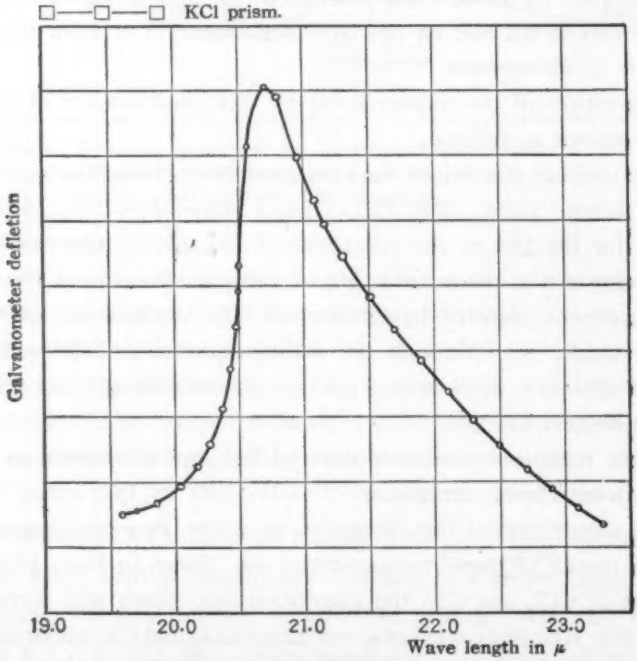

Fig. 8. Quartz residual ray.

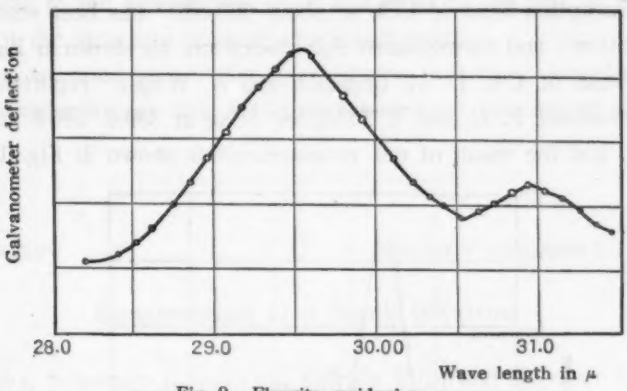

Fig. 9. Fluorite residual ray.

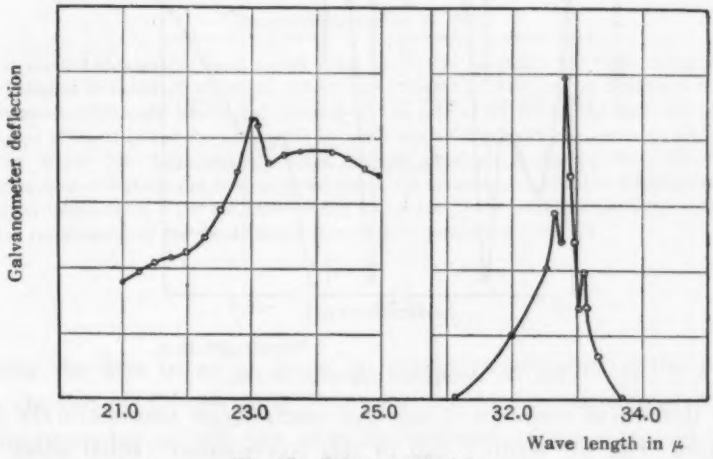

Fig. 10. Calcite residual ray.

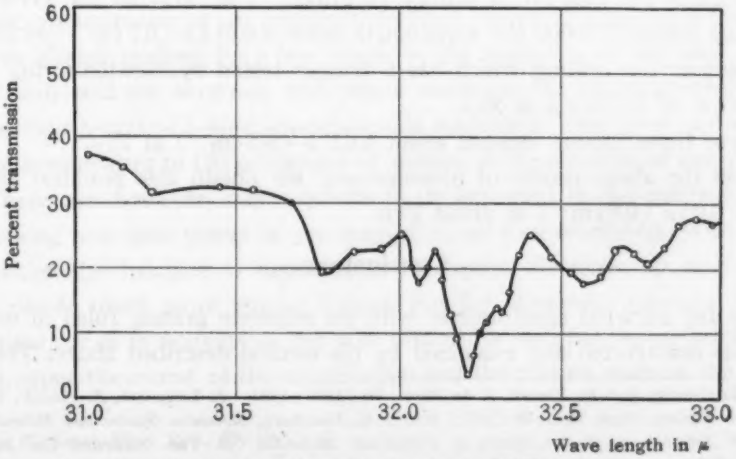

Fig. 11. Absorption spectrum of CCl_4.

The absorption band of CCl_4 at about 305 cm^{-1} has been reported by several investigators[5], and we measured this absorption, as shown in Fig. 11. For the absorption band of CS_2, D. M. Dennison and N. Wright[6] reported the envelope structure possessed P, Q and R branches lying at 389.4, 396.8 and 405.8 cm^{-1} respectively, and the result of our measurement is shown in Fig. 12.

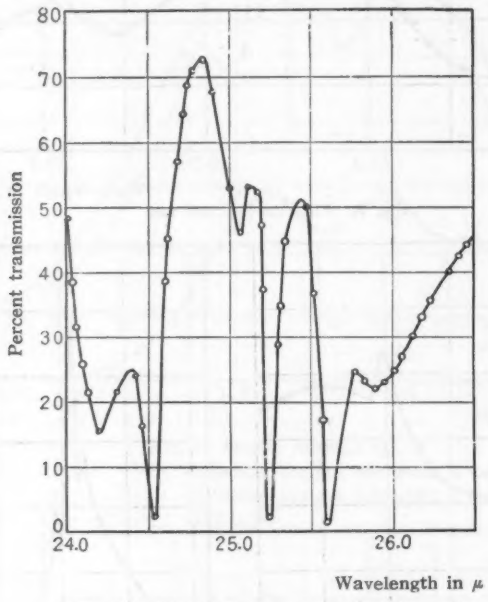

Fig. 12. Absorption spectrum of CS_2.

The theoretical resolution of this type spectrometer depends on the following three factors. The slit width 1 mm of this spectrometer (equal width for both slits) contains the interval of 0.014 μ (0.213 cm^{-1}) at 25 μ, by the error of the collimating mirror 1/10000 the wave-length error is 0.013 μ (0.2 cm^{-1}) at 25 μ, and the flatness of the grating which has 5 fringes tested by Newton's ring method causes error of 3×10^{-4} μ at 25 μ.

These three factors amount about 0.027 μ (0.5 cm^{-1}) at 25 μ.

From the above results of measurement we obtain the practical resolving power is 0.05 μ (0.8 cm^{-1}) at about 25 μ.

Conclusions

The far infra-red spectrometer with the echelette grating ruled in our laboratory was constructed and examined by the method described above. This spec-

5) P. Barchewitz and M. Parodi, J. de Phys., **10** (1939) 143; A. Langseth, Z. Physik, **72** (1931) 350; J. Strong, Phys. Rev., **38** (1931) 1818; G. Herzberg, *Molecular Spectra and Molecular Structure II. Infrared and Raman Spectra of Polyatomic Molecules*, (D. Van Nostrand Co. Inc., New York, 1949); 6) D. M. Dennison and N. Wright, Phys. Rev., **38** (1931) 2077.

tometer is useful to the wave-length about 35 μ or more and will be used for the investigation of the structure of molecules and crystals.

Moreover, we want to use this spectrometer to farther wave-length region, by means of evacuation of this whole instrument and increase of sensitivity of the detector.

SCIENCE OE LIGHT VOLUME 2, NUMBER 1 1952

Construction of a Small Betatron

Mitsuo MIWA, Seizaburo KAGEYAMA, Kiyoshi FUJII and Katsumi KURIYAMA.

Department of Physics, Tokyo University of Education

(Received December 4, 1951)

A small betatron having a stable orbit of 8.5 cm in radius has been constructed. The magnet is made of standard silicon steel sheets of 0.35 mm in thickness and is energized by 430-cycle alternating current at the rate of 90 KVA. The methods of the injection of electron and the expansion of orbit are substantially the same as are adopted by Kerst. The final energy of the electron obtained is about 3 Mev. The X-ray yield is also still poor and is equivalent about 150 milligrams radium in the direction of electron beam. Such a low electron energy and a low X-ray yield are probably ascribed to the ruggedness of our home-made pole pieces of magnet.

---

1 Introduction

Seeing the first paper of Kerst on betatron[1] published in the summer of 1941, we decided on the advice of Professor Yoshio Fujioka to construct a small one in the beginning of 1942, just after the outbreak of the war, and about two years later we had most of the essential parts of the machine at hand. Since the economic circumstances of our country thereafter, however, were not in our favour. our work almost stopped for a few years. In the beginning of this year we have at last completed the betatron, with which electrons can be accelerated up to 3 Mev, yielding X-rays of 2 Mev monochromatic equivalent. The X-ray output of the machine is equivalent to 150 milligrams of radium in the direction of electron beam.

There are, however, many defects to be improved in the machine. We are now making new pole pieces of the magnet in our own workshop. With the new pole pieces the machine is expected to accelerate electrons up to 5—6 Mev, giving rise to much more intense X-rays. But for economic reasons it will take much time for us to accomplish the pole pieces. So we shall report briefly in the present paper the course of the construction and the present state of the betatron.

1) D. W. Kerst, Phys. Rev., **60** (1941) 47.

2 The Magnet

Referring to the rough diagram given in Kerst's paper, we undertook to make a magnet of the same size as his. Kerst made his magnet of 0.003-inch (0.075 mm) silicon steel sheets. But we had no such thin silicon steel sheet. Thin sheets of course were desirable because we intended to energize the magnet with 500-cycle alternating current. The Yawata Iron Works was manufacturing 0.1 mm silicon steel sheets at that time. The product was, however, entirely given over to military service and there was no possibility of having even a few sheets. A detailed study therefore was made on the iron loss in standard silicon steel sheets of 0.35 mm in thickness at high frequencies. Fortunately the iron loss was shown not very high even at 1000 cycles. Thus we decided to make the magnet from standard sheets.

The next difficulty encountered in the construction of the magnet seemed much more serious for us. No one seemed willing to make the magnet for us. Even a small workshop was too busy on military service to accept our proposal. But one small shop fortunately complied to make the core of the magnet except for the two pole caps, which were too troublesome to make in a busy shop. We had the core in the beginning of 1943.

It was tedious work to make the pole caps. They were made of seven kinds of laminations of different breadth, the total number of laminations being about 1500 in each cap. No workshop took on such tedious work and we had to hand-cut the laminations with scissors. The laminations were arranged radially so that perfect circular symmetry was achieved at the pole faces. After Kerst, they were at first stuck together with a mixture of water glass and flint dust and hardened by baking. But the cement was found to be too frail mechanically. The laminations therefore were later held together with Bakelite varnish and wrapped with Japanese paper, although there was some danger of the softening of the cement due to the heat evolved in iron. After the war we knew that Kerst used thermo-setting resin as binding material in his second betatron[2].

With Bakelite varnish it was possible to stick the laminations much more easily and soundly than before. Yet the pole caps were not rigid enough for our purpose and were broken very often. It must be confessed that our pole caps were too thin to have sufficient mechanical strength. They were only 20 mm thick in the center and 6 mm in the periphery. We had chosen this thickness so that the acceleration chamber sandwiched with two pole caps could be easily inserted through between the two secondary coils. This trouble interrupted our work so frequently that we keenly felt the necessity of the reconstruction of the pole

2) D. W. Kerst, Rev. Sci. Inst., **13** (1942) 387;

pieces, although we sometimes observed the emission of weak X-rays from the machine with a G. M. counter[3]. But we could not afford to do this for economic reasons even after the end of war.

Referring to the papers on betatron received after the war, we reconstructed the magnet in the end of 1948, as shown in Fig. 2. The principal points of reconstruction were:

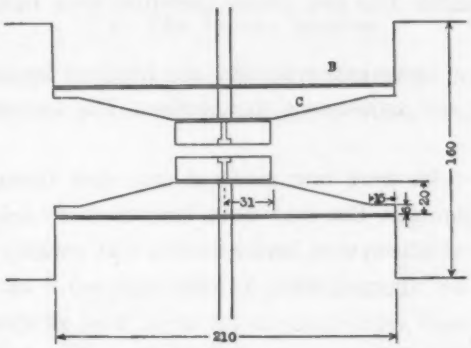

Fig. 1. The details of the central part of original magnet.

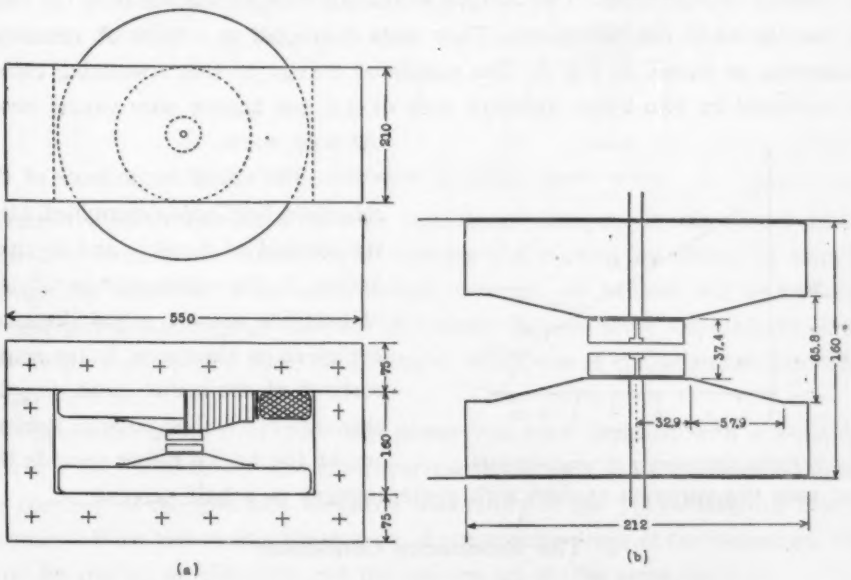

Fig. 2. (a) The present magnet. (b) Dimensions of pole pieces.

(1) The upper part of the yoke was cut off from the remainder so that it could be lifted by chain to mount the acceleration chamber with ease. The steel laminations of the yoke were clamped tightly with brass bolts running through

3) Y. Fujioka, M. Miwa, S. Kageyama and K. Fujii, Nippon Buturigakkaishi, 4 (1949) 78 (in Japanese).

the holes punched in the laminations.

(2) Pole pieces B were also cut off from the yoke and replaced by new pole pieces made of radially arranged laminations. The new pieces are equal in size to pole pieces B plus pole caps C of the original magnet (Fig. 1), and are about 6 cm in height. They were tightly bound with cotton tape, dipped in Bakelite varnish and baked. The new pieces therefore were rigid enough and were no more broken.

In consequence of these improvements, the machine became far more convenient in assemblage and adjustment than before. The vacuum system was also improved greatly.

The central flux disks were first made of iron dust through the courtesy of the Tôhoku Metal Company. But they were later made by being stacked parallel with different widths of silicon steel laminations so that roughly circular symmetry was achieved. They are approximately 14 mm high and 6 cm in diameter.

The secondary coils were made in the same way as was adopted by Kerst. One hundred strands of 0.9 mm enameled wire were made into a cable which was twisted several times. Two 19-turn secondary coils were made from the cable and were fitted to the pole pieces. They were connected to a bank of resonance condensers, as shown in Fig. 5. The supply of energy to this resonating circuit was achieved by two 9-turn primary coils of 2.4 mm copper wire wound about the pole pieces.

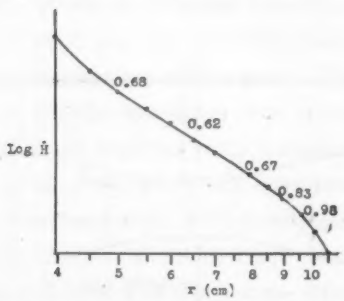

Fig. 3. Radial dependence of magnetic field.

The radial dependence of the magnetic field was determined after the method of Kerst[1] and is given in Fig. 3. The values of n in r^{-n} law of field for various radial distances are given on the curve. In the neighborhood of the stable orbit ($r=8.5$ cm), $H\sim r^{-0.72}$. The circular symmetry of the field is rather poor. In the worst case the variation of field with angle amounts to a half percent.

3 The Resonance Condenser

The next question faced in the beginning of our project was the dielectric hysteresis loss in the resonance condeser. Kerst used special condensers containing Piranol oil of high grade in his first betatron. No such condenser, however, was at our disposal. The Tokyo-Shibaura Electric Company was manufacturing Shibanol oil of the same quality as Piranol at that time, but all the product was again devoted to the military service and we had to be contented with ordinary

power condensers. Fortunately there was found no trouble in the operation of ordinary condensers at 500 cycles. They worked safely even without any special cooling device.

The present condenser bank consists of 15 units of various characters that happened to be at hand, the total capacity of which is 63 microfarads.

4 The Power Source

In the early stage of our project in 1944—1945 the magnet was energized with a 1-kilowatt thyratron inverter, the circuit of which is shown in Fig. 4. The

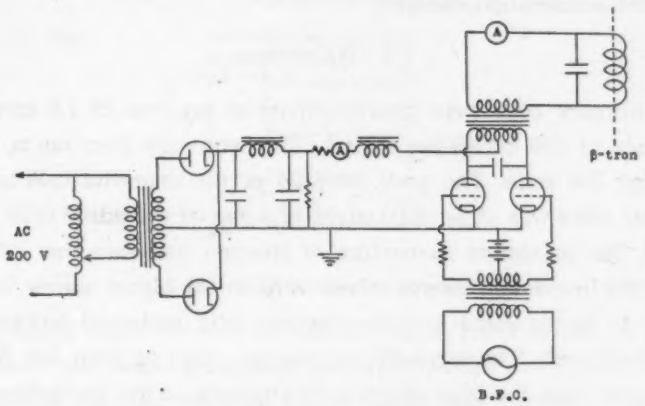

Fig. 4. Wiring diagram of the original power source.

thyratron inverter has an advantage capable of changing the frequency freely. With this inverter we succeeded in running the current up above 50 amperes through the secondary coils. A 3-kilowatt inverter, we believe, will be sufficient for energizing our magnet. But the thyratron did not work smoothly in winter without the regulation of room temperature, which was of course almost impossible in the wartime.

Since the autumn of 1945 the power has been supplied with a 3-kilowatt 500-cycle alternator driven by a direct-current motor with adjustable speed, through the courtesy of the Matsuda Research Laboratory of the Tokyo-Shibaura Electric Company. With this source the r. m. s. electromotive force in the secondary coils could be run up to 800 volts and the current up to 150 amperes.

5 The Acceleration Chamber

In the beginning of the project, we succeeded in making a doughnut-shaped acceleration chamber from glass. But with the progress of the war, it became very difficult to have a new chamber. A porcelain chamber with glazed surface therefore was made and has been successfully used until recently. Kerst also used

a porcelain chamber in his 80 Mev betatron[4]. Recently we have again replaced the porcelain chamber by a glass one, because the latter has several advantages.

A hard glass tube of 4 cm in diameter was bent into semicircular form. Two such semicircular pipes were made and joined together to form a doughnut-shaped chamber. The outer diameter of the chamber is 20 cm and the center of the doughnut is 9 cm in diameter.

The injector was made of 0.15 mm molybdenum sheets and a spiraled tungsten filament, the assembly and dimension of which were nearly the same as those of 80 Mev betatron of Illinois. It was placed at the distance of 93 mm from the center of the acceleration chamber.

6 Operation

The primary coils were usually driven at the rate of 1.8 kilowatts and at the frequency of 430 cycles per second. The secondary then ran at 90 KVA, the voltage being 700 volts. The peak intensity of the magnetic field at the surface of the center piece was about 6000 gauss and that at the stable orbit ($r=8.5$ cm) 1400 gauss. The maximum momentum of electron therefore was 12000 gauss-cm in $H\rho$ and the maximum energy about 3 Mev. At higher power input the iron core began to be saturated and the electron orbit collapsed before the highest energy was attained. The saturation of the iron core at such low field intensity seems to come from the high effective flux density in the laminations due to the low space factor in our hand-made pole pieces. New pole pieces of high space factor are now in preparation.

The adjustment of the position of the stable orbit was again performed after the method of Kerst; namely, rough adjustment by changing the thickness of the center pieces and fine adjustment by inserting a thin sheet of paper between the upper bar and the remainder of the yoke.

Electrons were usually injected at about 10 kilovolts. The X-ray yield decreased with decreasing injection voltage and went down to a half intensity at about 7 kilovolts. The continuous injection of electrons caused gradual sputtering of the silver coating of the acceleration chamber and also liberation of gas from the chamber wall, resulting in a drop of X-ray yield. Electrons therefore were injected impulsively for approximately 20 microseconds with the circuit shown in Fig. 5. A permalloy strip with a coil wound about it was placed between the center pieces. This strip is saturated most of the time and generates a triggering voltage in the coil at the instant when the main field goes through zero, starting the injector[2]. The timing of injection can be shifted by an adjustable timing circuit inserted as shown in Fig. 5.

4) D. W. Kerst, G. D. Adams, H. W. Koch and C. S. Robinson, Rev. Sci. Inst., 21 (1950) 462.

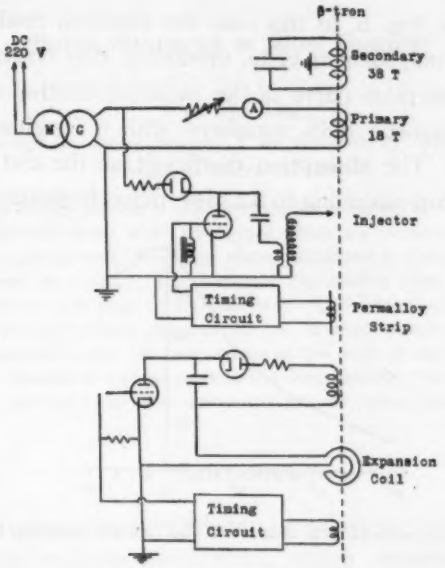

Fig. 5. The injection and orbit expansion circuits.

The accelerated electrons were at first allowed to move inward to a smaller radius of curvature and finally graze past the target placed inside the stable orbit as the saturation of the core went on at the higher field intensity. The electron orbit is now made to expand outward at a desired phase of field by means of a pair of expansion coils[2] placed directly above and below the doughnut, the wiring

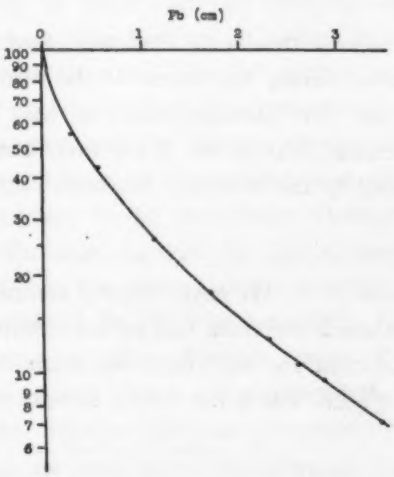

Fig. 6. Absorption by lead, of X-rays generated by the electrons which were made to expand at about 80° phase angle of magnetic field.

of which is shown in Fig. 5. In this case the electrons finally strike the injector on the back of the molybdenum plate, producing thin target X-rays.

Fig. 6 is an absorption curve of the radiation emitted at the phase angle of about 80° of the magnetic field, measured with a Lauritsen electroscope, as it passes through lead. The absorption coefficient at the end of the curve is 0.49 cm^{-1} Pb, the value corresponding to 2.1 Mev monochromatic equivalent. In Fig. 7

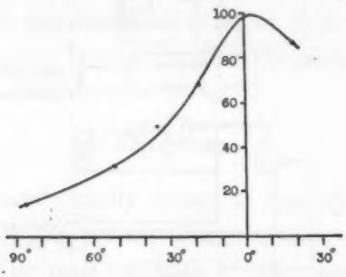

Fig. 7. Angular dependence, with respect to the incident electron beam, of the same X-rays as in Fig. 6.

is shown the angular distribution of the radiation with respect to the incident electron beam, which gives a half-value angular breadth of about 64°. This is in good agreement with the theoretical volue[5] 64° for thin target bremsstrahlung generated by 2.7 Mev electron.

The X-ray yield was rather poor in the early stage and was equivalent to a few milligrams of radium. But the yield later attained to about 150 milligrams radium equivalent in the direction of electron beam.

We express our hearty thanks to Professor Yoshio Fujioka for his kind advice and encouragement during the course of the work. We are also indebted to Dr. Shigeru Mita and Mr. Mashige Nagai of the Tokyo-Shibaura Electric Company for their technical helps given in the early stage of the work.

The work was aided by the Scientific Research Expenditure of the Ministry of Education.

Note added in proof: —— We have recently completed new pole pieces of high space factor, with which electrons can be accelerated up to 6 Mev. But our power source is not sufficient for such high excitation. At present we can accelerate electrons up to 4 Mev. The X-ray output is equivalent to about one gram radium.

5) L. I. Shiff, Phys. Rev., **70** (1946) 87; J. D. Lawson, Proc. Phys. Soc., A **63** (1950) 653.

Pulse Shape of a Slow Counter

Ryumyo ITO

Institute for Optical Research, Tokyo University of Education

(Received March 15, 1952)

The pulse shape of a slow counter is calculated on the assumption that a complete discharge of a slow counter consists of many small discharges which are carried out one after another by the secondary emission at the wall. The pulse shape calculated is quite similar to the observed one; both of them show, as a whole, approximately exponential rises, but, in detail, look like stairs, and the duration of each step of the stair is nearly the same with the calculated transit time of the ions. The pulse shape depends on the counter circuit. We can expect the best characters of a slow counter when the capacitance of the wire system is diminished as much as possible. The leak resistance has an optimum value, because the higher one makes the resolving time longer and the lower one makes the plateau range narrawer.

1 Introduction

Geiger counters are often divided into two classes—namely, fast counters and slow counters. A fast counter has a filling which contains polyatomic gas, and its discharge is quenched by internal mechanism; therefore it is sometimes called a *self-quenching counter*. On the contrary a slow counter has a filling which contains merely diatomic gas or monoatomic gas, and its discharge can not be quenched unless it is helped by some external quenching circuit; it is sometimes called a *non self-quenching counter*.

As a fast counter has much better qualities than a slow counter — namely, a far wider plateau range and better reliability — it has been studied very well since it was first made by Trost[1], and its discharge mechanism is now fairly clear. Although a slow counter has longer history than a fast counter, its discharge mechanism is not yet clear. Werner[2] carried out extensive experiments for slow counters and explained the discharge mechanism as a not self-sustaining corona discharge. He measured the lifetime of the corona discharge and its dependence on the overvoltage of the counter, and found that the lifetime is proportional to the exponent of the overvoltage. Duffendack[3] also took the minimum self-sustaining discharge current for the measure of reliability of the counter. He concluded that the plateau range is nearly equal to minimum self-sustaining current multiplied by the leak resistance. Kita[4] observed the pulse shapes of a slow counter on an oscilloscope screen. He proposed the *ion cloud theory* instead of the *ion sheath theory*, and explained the properties of the pulse shape — e.g. the height, the rise time, etc., considering the internal resistance

1) A. Trost, ZS. f. Phys., **105** (1937) 399; 2) S. Werner, ZS. f. Phys., **90** (1934) 384, **92** (1934) 705; 3) O. S. Duffendack, H. Lifschutz and M. M. Slawsky, Phys. Rev., **52** (1937) 1231; 4) I. Kita, Jour. phys. Soc. Japan, **6** (1951) 99.

of the counter to be constant. C. G. Montgomery and D. D. Montgomery[5] suggested, however, that the discharge mechnism of a slow counter is practically the same as that of a fast counter except the fact that, in a slow counter, many stages of the successive discharge are caused by the secondary electrons emitted from the cathode by positive ion impact.

The author agrees with Montgomey's idea, and will calculate, in this paper, the pulse shape of a slow counter along the line suggested by Montgomery, and will compare the dependence of the characteristics of the calculated pulses on the external circuit with that of the observed ones.

2 Discharge mechanism of a slow counter

The discharge mechanism of a fast counter is considered as follows: When an ionization takes place in the counter, the liberated electron is accelerated toward the central wire, and ionizes the gas molecules by collision in case the electric field is strong enough in the neighbourhood of the wire. Electrons emitted by collisions can become origins of successive ionization, and thus there occurs a cascade process of ionization, an avalanche. During this process, ultraviolet rays are also emitted, which cause other avalanches at some places apart from the first avalanche, and the discharge spreads over the counter. Since the ions produced in this process have smaller mobility as compared with electrons, they remain practically in the vicinity of the central wire during the growth of discharge. The space charge increases gradually and shields the strong field near the central wire. The avalanche formation thus stops. The ion sheath moves then slowly toward the cathode and the potential difference drops. As there is no secondary electron emission in a fast counter, the discharge finishes completely in only one step of discharge.

We assume, for the discharge mechanism of a slow counter, that an ion sheath is formed in the same way as in a fast counter, and that the discharge stops once. We shall provisionally call this process an elementary discharge. We also assume, however, that some new electrons which can cause another elementary discharge are born by impact of the ion layer with the cathode, and that those processes are repeated successively. If a high resistance is inserted in the counter circuit, the charge that flows into the electrodes of the counter through the resistor during one stage of the elementary discharge is not sufficient to maintain the counter voltage. The counter voltage thus drops step by step. Since the average number of the secondary electrons ejected by an impact of the ion layer must be proportional to the number of the positive ions which are again nearly proportional to the overvoltage of the counter, the secondary electrons

5) C. G. Montgomery and D. D. Montgomery, Phys. Rev., 57 (1940) 1030.

also decreases by steps. If no electron is ejected by an impact of the ion layer at some stage, the following elementary discharge can not occur, and thus the dicharge train terminates. A discharge of a slow counter is completely finished and a pulse is formed.

Why we consider that the discharges of a slow counter are quenched by an ion space charge just as a fast counter is based upon the following reasons: To take place a continuous discharge in a counter, the positive ions generated by Townsend discharges must be swiftly removed from the discharging zone, or the field strength in it will be weakened by the charge of the ions. If we compare an argon-filled counter with an argon-alcohol mixture filled one, for a typical example of the slow and the fast counter respectively, we find the mobilities of these ions are not so much different; the mobilities of the argon ion and the alcohol ion are 1.4 cm/sec/volt/cm and 0.38 cm/sec/volt/cm respectively[6], and the mobility of the alcohol ion in argon alcohol mixture will be larger than that in pure alcohol vapor. In a slow counter, moreover, the discharge propagates more rapidly than in a fast counter on account of the photoelectric emission from the cathode during the Townsend discharge. It is most reasonable, therefore, that an ion sheath is formed in a slow counter just as in a fast counter.

It is very clear from various experiments[7] that the secondary emission from the cathode is existent in a slow counter, while it scarcely exists in a fast counter. Why the secondary emission is suppressed by the addition of polyatomic gas has been discussed by Korff and Present[8] and has been proved by many experimental facts. There are two kinds of electron emission from the cathode in a slow counter—namely, photoelectric emission and secondary emission by ion impact. Among these cathode effects, photoelectric emission promotes the growth of the discharge because photoelectrons are generated in a negligibly small time after the original discharge. The propagation velocity of the discharge along the wire is greater and the rise time of the pulses is shorser in a slow counter than those in a fast counter[9]. The secondary emission by ion impact ocurrs after the ions reach the wall (it takes about 10^{-4} sec), and therefore, the electrons cause a new elementary discharge if the field near the wire is already recovered.

In a fast counter, the charge contained in an ion sheath is nearly proportional to its overvoltage. Let q be the charge of the ion sheath per unit length. According to Wilkinson's calculation[10], it may be written as follows for a counter at a small overvoltage:

$$q=\varphi c^2\eta V_0(V_0-V_s), \tag{1}$$

6) *International Critical Table*, Vol. VI, p. 111, McGraw Hill Co. (1929); 7) M. E. Rose and S. A. Korff, Phys. Rev., **59** (1941) 850; 8) S. A. Korff and R. D. Pre- sent, Phys. Rev., **65** (1944) 274; 9) D. R. Corson and R. R. Wilson, Rev. Sci. Inst., **19** (1948) 207; 10) D. H. Wilkinson, Phsy. Rev., **75** (1948) 1417.

where φ: a characteristic constant of the counter with its value usually 4~20,
c: the electrostatic capacitance of the counter per unit length,
η: the ionization coefficient (per volt) by collision of electrons for the filling,
V_0: the counter voltage at the beginning of the discharge,
V_s: the threshold voltage for Geiger discharge.

We may expect that the charge included by an ion sheath at each stage of elementary discharge in a slow counter can be also represented by the above formula.

Let s be the number of secondary electrons ejected by an impact of the ion layer in a slow counter, and $\bar{s}$ be the average value of s. Since $\bar{s}$ is proportional to the number of ions included in the ion layer, it is represented as follows:

$$\bar{s}=\frac{q\gamma}{e}\propto V_0-V_s, \tag{2}$$

where γ is the probability of the secondary emission per impact of an ion, and e is the elementary charge. If the overvoltage decreases with the progress of discharges, the average number of the secondary electrons decreases accordingly. If $s=0$ occurs once, the next elementary process cannot appear, and the discharge train terminates. As s shows a statistical fluctuation, $s=0$ can occur even for a pretty large $\bar{s}$.

The value of γ has never reported, so far as we know, but from our theoretical estimation in a hydrogen-filled counter γ seems to be of the order of 10^{-7}. For glow discharge between parallel plate electrodes, the coefficient of the secondary emission is reported nearly to be 10^{-2}~10^{-3} [11]; it includes, however, the factor by the photoelectric emission, and the coefficient of secondary emission by ion impact will be far smaller than this value. In a fast counter γ must be negligibly small.

We assume that the mobility of ion κ can be define as a constant. Strictly speaking, κ must be a function of the radial coordinate, because the field strength at the position of an ion in a counter changes extremely on the way from the anode to the cathode. It seems, however, that above assumption does not lead any essential error into the properties of pulses.

We also assume that the ion sheaths are formed very near the wire, and that the burning time is negligibly small as compared with the transit time of the ion layer.

3 Elementary discharge

We now consider the first elementary discharge in a counter at small overvoltage. In this case

11) L. B. Leob, *Fund. Proc. of Elec. Discharge in Gases*, p. 392, John Wiley and Sons Co. (1939).

$$V_0 > V_s, \tag{3}$$

$$V_0 - V_s < V_s, \tag{4}$$

where V_0 is the initial counter voltage, and V_s is the threshold voltage for Geiger discharge. We show schematically a Geiger counter and its circuit in Fig. 1. Suppose that a discharge occurs at the time $t=0$, and that the ion sheath is at the distance r from the wire when $t=t$. We express the charge included in the sheath formed by the discharge per unit length by q, and that distributed on the cathode per unit length by $-Q$; then the charge distributed on the wire is

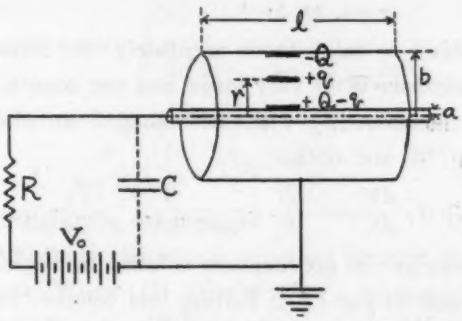

Fig. 1. Schematic diagram of a slow counter and its circuit.

$Q-q$ (neglecting the end effect). We denote the radii of the wire and the cathode by a and b respectively; then the electrostatic capacitance between the wire and the cathode per unit length is represented by

$$C=\frac{1}{2\ln(b/a)}. \tag{5}$$

Let κ be the mobility of the ions, and X be the field strength at the position of the ion layer. We assume here that X is equal to the mean value of the field strength at the front and the back surfaces of the ion layer. Then,

$$X=(2Q-q)/r.$$

The radial velocity of an ion is

$$\frac{dr}{dt}=\kappa X=\frac{\kappa(2Q-q)}{r},$$

or

$$\frac{d}{dt}(r^2)=2\kappa(2Q-q).$$

Put $r^2/a^2=S$, then,

$$\frac{dS}{dt}=\frac{2\kappa(2Q-q)}{a^2}. \tag{6}$$

If the cathode is grounded, the wire potential at $t=t$ is shown by

$$V=\frac{Q}{c}-q\ln S \tag{7}$$

Let C be the external capacitance connected to the wire, l be the length of the

counter and R be the leak resistance; then we can get the following equation from Kirchhoff's law for current, as is evidently on Fig. 1

$$l\frac{dQ}{dt}+C\frac{dV}{dt}=\frac{V_0-V}{R}. \tag{8}$$

We have to integrate the equations (6), (7) and (8) to obtain S, Q and V as functions of t. The initial conditions are

$$\left.\begin{aligned} &V=V_0\\ &Q=cV_0\equiv Q_0\\ &r=a, \text{ or } S=1 \end{aligned}\right\} \text{ when } t=0. \tag{9}$$

As it is fairly difficult to solve them accurately, we consider only the cases in which the leak resistance R is very large and the counter overvoltage is small. Since r increases monotonously with increasing t, we eliminate t and Q from Eqs. (6), (7), and (8), and obtain

$$(C+cl)\frac{dV}{dS}=-\frac{qcl}{S}+\frac{a^2(V_0-V)}{2\kappa R(2cV-q+2qc\ln S)}. \tag{10}$$

If R is large, we can get an approximate solution by neglecting the second term of the right hand side of Eq. (10). Putting this solution into the neglected term of Eq. (10), we get the second approximate solution, and so on.

The first approximate solution is

$$V=V_0-\frac{qcl}{C+cl}\ln S. \tag{11}$$

The second approximate equation becomes

$$\frac{dV}{dS}=-\frac{qcl}{(C+cl)S}+\frac{a^2qcl\ln S}{2\kappa R(C+cl)^2\left(2cV_0-q+\dfrac{2qcC}{C+cl}\ln S\right)}, \tag{12}$$

and this solution is

$$V=V_0-\frac{qcl}{C+cl}\ln S+\int_1^S\frac{a^2qcl\ln S\,dS}{2\kappa R(C+cl)^2\left(2cV_0-q+\dfrac{2qcC}{C+cl}\ln S\right)}. \tag{13}$$

If the overvoltage is small,

$$q\ll Q_0,$$

and we get

$$V=V_0-\frac{qcl}{C+cl}\ln S+\frac{a^2ql(S\ln S-S+1)}{4\kappa RV_0(C+cl)^2}. \tag{14}$$

When the ion layer reaches the cathode,

$$\ln S=\frac{1}{c},$$

and

$$V\approx V_0-\frac{ql}{C+cl}\left\{1-\frac{b^2}{4\kappa RV_0(C+cl)}\left(\frac{1}{c}-1\right)\right\}. \tag{15}$$

Next we consider the position of the ion layer as a function of t; i. e. we try to integrate the equation (6). We use here the first approximate value (11) for V. Putting Eq. (11) into Eq. (6), we get

$$\frac{dS}{dt}=\frac{2\kappa}{a^2}\left(2cV_0-q+\frac{2qcC}{C+cl}\ln S\right),$$

or

$$t=\int_1^S \frac{a^2dS}{2\kappa\left(2cV_0-q+\frac{2qcC}{C+cl}\ln S\right)}. \tag{16}$$

The transit time of the ion layer is

$$\tau=t_{S=a^2/b^2}=\int^{b^2/a^2} \frac{a^2dS}{2\kappa\left(2cV_0-q+\frac{2qcC}{C+cl}\ln S\right)}. \tag{17}$$

Especially for small overvoltage, τ becomes

$$\tau=\frac{a^2}{4\kappa cV_0}\left(\frac{b^2}{a^2}-1\right)\approx\frac{b^2}{4\kappa cV_s}. \tag{18}$$

τ is nearly independent of the overvoltage.

The field strength near the wire is uniquely decided by the charge $(Q-q)$ distributed on the wire. When $(Q-q)$ is over cV_s, a new discharge can start, and when $(Q-q)$ is under cV_s, any new discharge can not occur.
Put $V=V_0-v$, then,

$$v\geqq 0.$$

Using the Eq. (7), we get

$$\begin{aligned} Q-q&=cV+qc\ln S-q\\ &=cV_0-q+qc\ln S-cv\\ &\leqq cV_0-q+qc\ln S. \end{aligned} \tag{19}$$

Since the deduction of Eq. (19) implies no approximation, Eq. (19) is independent of the overvoltage and the leak resistance. Therefore the counter is always inactive until the ion layer arrives at the distance r' described as follows:

$$cV_s=cV_0-q+qc\ln(r'^2/a^2)$$

or

$$r'=a\exp\left(\frac{1}{2c}-\frac{V_0-V_s}{2q}\right)=b\exp\left(-\frac{V_0-V_s}{2q}\right). \tag{30}$$

Since q is approximately proportional to the overvoltage as shown in Eq. (1), r' does not depend upon the overvoltage. This agrees with Stever's theory[12].

In Fig. 2 we show the change of the wire potential V calculated from Eqs. (14) and (16), together with that of the field strength near the wire X_a. For this calculation we give the following appropriate values to the constants of a counter:

$a=0.01$ cm,	$\varphi=5$,	$V_s=1000$ volt,
$b=1.5$ cm,	$\eta=0.01$ volt^{-1},	$V_0=1010$ volt.

12) H. G. Stever. Phys. Rev., **61** (1942) 38.

$l=10$ cm, $\kappa=100$ cm/sec/volt/cm,

These values correspond to a hydrogen filled counter used in usual experiments. For the value of C, we chose zero and 10 cm, and for R we give various values. For $C=10$ cm, we can see that when the ion layer reach the cathode the wire potential is still higher than the threshold value V_s even with $R=\infty$, and that the field near the wire is strong enough to cause next Geiger discharge.

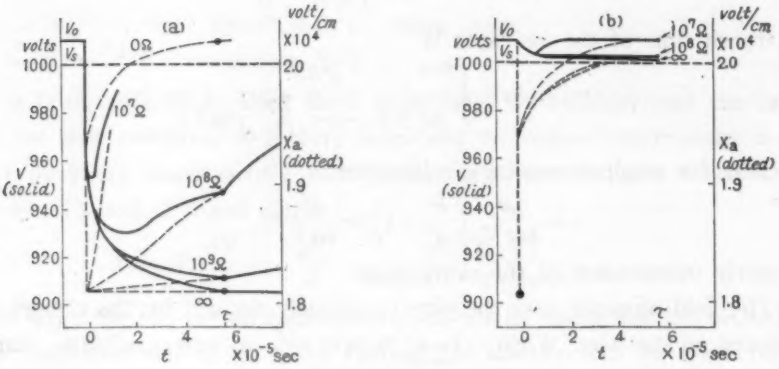

Fig. 2. The wire potential V and the field strength near the wire X_a as functions of time t. The ion sheath reaches the cathode when $t=\tau$.
(a) $C=0$, (b) $C=10$ cm.

4 Successive discharge

If the field in the counter recovered strong enough to cause a Geiger discharge, the secondary electrons emitted by ion layer impacts with the cathode cause a next new elementary discharge, and thus many discharges follow successively.

We now consider the wire potential when the n-th ion layer is moving between the electrodes. Let V_n be the wire potential at the beginning of the n-th discharge, and q_n be the charge included in the n-th ion layer per unit length of the counter; then we get the following equation by the same way as for Eq. (10);

$$(C+cl)\frac{dV}{dS}=-\frac{q_n cl}{S}+\frac{a^2(V_0-V)}{2\kappa R(2cV-q_n+2q_n c\ln S)},$$

or

$$\frac{dV}{dS}=-\frac{q_n cl}{(C+cl)S}+\frac{a^2(V_0-V_n)}{2\kappa R(C+cl)(2cV-q_n+2q_n c\ln S)}+\frac{a^2(V_n-V)}{2\kappa R(C+cl)(2cV-q_n+2q_n c\ln S)}. \tag{21}$$

If R is large, the change of the wire potential in the transit time of the n-th

ion layer is given using Eq. (13) as follows:

$$\delta V_n=-\frac{q_n cl}{C+cl}\cdot\frac{1}{c}+\frac{V_0-V_n}{R(C+cl)}\int_1^{b^2/a^2}\frac{a^2dS}{2\kappa(2cV_n-q_n+\dfrac{2q_ncC}{C+cl}\ln S)}$$

$$+\frac{1}{2\kappa R(C+cl)^2}\int_1^{b^2/a^2}\frac{a^2q_ncl\ln SdS}{2cV_n-q_n+\dfrac{2q_ncC}{C+cl}\ln S}. \tag{22}$$

We neglect the third term of the right hand side because it is far smaller than the second term for large n. The integral in the second term is equal to the transit time τ_n from Eq. (17), and we get, therefore,

$$\delta V_n=-\frac{q_nl}{C+cl}+\frac{(V_0-V_n)\tau_n}{R(C+cl)}. \tag{23}$$

For small overvoltage, we have from Eq. (1)

$$q_n=\varphi c^2\eta V_n(V_n-V_s)\approx gV_s(V_n-V_s), \tag{24}$$

where
$$g=\varphi c^2\eta, \tag{25}$$

and from Eq. (18)

$$\tau_n=\tau=\frac{b^2}{4\kappa cV_s}. \tag{26}$$

Therefore,

$$\delta V_n=-\frac{V_n-V_s}{C+cl}(glV_s+\frac{\tau}{R})+\frac{(V_0-V_s)\tau}{R(C+cl)}. \tag{27}$$

If n is large, we may integrate Eq. (27) regarding n, and we get the following formula putting $n\tau=t$.

$$V(t)=V_s+\frac{glV_s\exp\left\{-\dfrac{t}{\tau}\left(\dfrac{glV_s+\tau/R}{C+cl}\right)\right\}+\dfrac{\tau}{R}}{glV_s+\tau/R}(V_0-V_s). \tag{28}$$

If R is iarge ($R\gg\frac{\tau}{glV_s}$), this becomes

$$V(t)=V_s+(V_0-V_s)\exp\left\{-\frac{tglV_s}{\tau(C+cl)}\right\}. \tag{29}$$

We can see that the overvoltage as a whole decreases exponentially with time, and that its time constant is

$$T_r=\frac{(C+cl)\tau}{glV_s}. \tag{30}$$

When the leak resistance is large, the rise time of pulses is nearly independent of the overvoltage. As we see from Eqs. (27) and (28), δV_n decreases with increasing n. If R is not infinitely large, however, δV_n becomes zero at the following voltage V', and V cannot decrease below this value.

$$V'=V_s+\frac{(V_0+V_s)\tau}{glRV_s+\tau}. \tag{31}$$

If we assume that the number of secondary electrons emitted by a single impact of an ion layer conforms to Poisson's distribution, the probability of the occurence of the emission of s electrons is

$$p(s)=\frac{\bar{s}^s e^{-\bar{s}}}{s!}, \tag{32}$$

and that of an emissionless impact is

$$p(0)=\exp(-\bar{s}), \tag{33}$$

where $\bar{s}$ is the average value of s. The probability that the actual n-th elementary discharge accompanies no emission, is

$$P_n=(1-p_1)(1-p_2)\cdots\cdots(1-p_{n-1})p_n,$$

where p_n is the simple probability of emissionless impact of the n-th ion layer. Using Eqs. (2) and (24), we get

$$P_n=\exp\left\{-\frac{gl\gamma V_s(V_n-V_s)}{e}\right\}, \tag{34}$$

where V_n-V_s is found from Eq. (29). If $s=0$ once occurs, the discharge train terminates. This happens, on the average, at the m-th stage, where m is given by the following equation:

$$m=\frac{\sum_{n=1}^{\infty} np_n \prod_{l=0}^{n-1}(1-p_l)}{\sum_{n=1}^{\infty} p_n \prod_{l=0}^{n-1}(1-p_l)}, \tag{35}$$

where $p_0=0$.

Now we consider the following two limiting cases: (A) R is large and $(C+cl)$ is small, and consequently p_n increases steeply with increasing n. (B) R is small, or $(C+cl)$ is large, and p_n remains nearly constant in spite of the increase of n.

In the case (A), we may put $p_m=1$. The cut-off condition is

$$\exp\left\{-\frac{gl\gamma V_s(V_c-V_s)}{e}\right\}=1,$$

or

$$V_c=V_s+\frac{e}{gl\gamma V_s}. \tag{36}$$

where V_c is the wire potential at the last stage of the elementary discharges. If $V'\geqq V_c$, the discharge train cannot be cut off. The necessary condition to avoid lasting discharge is, therefore,

$$V'<V_c,$$

$$R>\frac{\tau}{glV_s}\left\{\frac{glV_s\gamma(V_0-V_s)}{e}-1\right\}. \tag{37}$$

Let T be the duration of the whole discharge; then we get from Eq. (28)

$$T=\frac{R(C+cl)\tau}{glRV_s+\tau}\ln\left\{\frac{V_c-V_s}{V_0-V_s}\left(1-\frac{\tau}{glRV_s}\right)-\frac{\tau}{glRV_s}\right\}^{-1}. \tag{38}$$

Especially for $R=\infty$,

$$T=\frac{(C+cl)\tau}{glV_s}\ln\left(\frac{V_0-V_s}{V_c-V_s}\right)=\frac{(C+cl)\tau}{glV_s}\ln\frac{gl\gamma V_s(V_0-V_s)}{e}. \tag{39}$$

In this case, the discharging duration is proportional to the logarithm of the overvoltage, and is also proportional to the external capacitance C if $C\gg cl$.

In the case (B), we get the following equation putting $p_1=p_2=\cdots\cdots=p_n=p$.

$$m=\frac{\sum_{n=1}^{\infty}np(1-p)^{n-1}}{\sum_{n=1}^{\infty}p(1-p)^{n-1}}=\frac{1}{p}. \tag{40}$$

The dicharge duration is, therefore,

$$T=m\tau=\tau\exp\left\{\frac{gl\gamma V_s(V_0-V_s)}{e}\right\}. \tag{41}$$

In this case. T is proportional to the exponent of the overvoltage and is independent of the leak resistance or the capacitance of the wire system. The discharge train is cut off by chance, and the discharge duration may show a large fluctuation.

In actual cases, the discharge duration must show some behaviors which are medium of the two limiting cases above discussed.

5 The pulse shape after the cut-off of the discharge train

After the cut-off of the discharge, the wire potential is changed only by the charge which has flowed into the counter through the leak resistor. Let V_t be the wire potential and t_t be the time when the latest ion layer arrives at the cathode; then we find

$$(C+cl)\frac{dV}{dt}=\frac{V_0-V}{R},$$

and

$$V_{t-}t_t=V_t,$$

hence,

$$V=V_0-(V_0-V_t)\exp\left\{-\frac{t-t_t}{R(C+cl)}\right\}. \tag{42}$$

The time constant of the recovering change is given by

$$T_t=R(C+cl). \tag{43}$$

In the limiting case (A), the pulse height is (V_0-V_c). Since the overvoltage at the moment of the cut-off is of the order of a few volts, (V_0-V_c) is nearly equal to (V_0-V_s). We may say, therefore, the pulse height is equal to the initial overvoltage.

In a slow counter, each pulse is formed by many successive elementary discharges, and it is impossible to count one or more primary ionizing events which happen during the discharge train. It is possible, however, to count an ionizing

event happen just after the cut-off of the discharge train. The dead time of a slow counter equals, therefore, the duration of the discharge train.

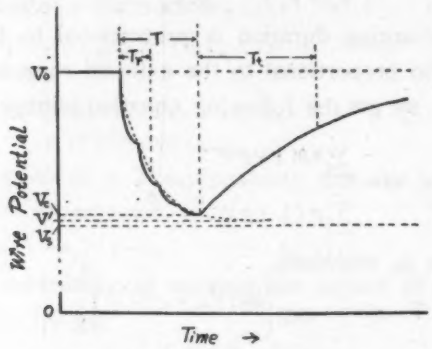

Fig. 3. Theorectical pulse shape.

The leak resistance must be very high in a slow counter circuit, and the recovering time is, therefore, very long. This makes the pulses smaller and at random in spite of not so high a counting rate.

The pulse shape (of the case (A)) above discussed is shown schematically in Fig. 3.

6 Experimental observations

Kita[4] has reported on the pulse shapes of a slow counter observed on the screen of a cathode ray oscilloscope. We also have made observations similar to his, but studied the pulse at the small overvoltage in detail.

The counter used has a cathode made of brass, which is 15 mm in diameter and 60 mm long, and has an anode of tungsten wire which is 0.20 mm in diameter. The fillings of the counters are argon or hydrogen. Hydrogen used was made by electrolysis and preserved in a vessel containing P_2O_5 powder for dehydration.

For accurate observation of the pulse shapes, we constructed a wide band amplifier and used a Johnson's quenching circuit[13] with it. To used a high leak resistance as the quenching circuit, and to apply the voltage drop on the resistor to the deflection plates of the oscilloscope is the best way to make accurate observation of the pulse shapes, but it is difficult to observe them over a wide range of the pulse height. To use a vacuum tube quenching circuit like Neher-Harper[14], Neher-Pickering[15], or Johnson circuits is equivalent to using a high resistance which is equal to the grid leak resistance multiplied by the amplifica-

13) T. H. Johnson, Rev. Sci. Inst., 9 (1938) 218; 14) H. V. Neher and W. W. Harper, Phys. Rev., 49 (1936) 940; 15) H. V. Neher and W. H. Pickering, Phys. Rev., 53 (1938) 316.

tion of the circuit, as shown by Fujioka, Kita, and Minakawa[16]. Especially Johnson circuit using a triode tube has an amplification independent of the counter voltage, and it is, furthermore, easier than the others to diminish the load resistance in order to get good response at high frequencies because of its low B voltage.

The quenching circuit and the amplifier circuit used are shown in Fig. 4, and the frequency response is shown in Fig. 5.

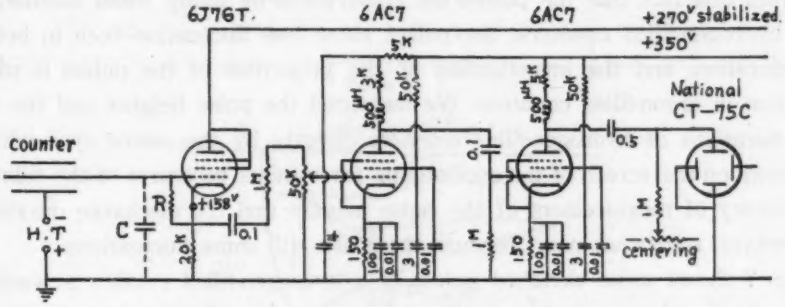

Fig. 4. The quenching circuit and the amplifier circuit.

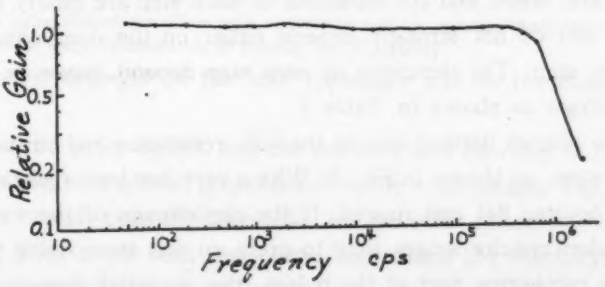

Fig. 5. The frequency response of the quenching circuit and the amplifier circuit.

Fig. 6. Some typical examples photographed of the pulse shapes of an argon-filled counter. (Pressure: 100 mmHg)

16) G. Fujioka. I. Kita and O. Minakawa. Jour. Phys. Soc. Japan. 6 (1951) 95.

Fig. 6 are some photographs which show typical pulse shapes of an argon-filled counters. In argon-filled counters the pulse shapes were easily photographed in detail, but we failed to photograph the pulse shapes in hydrogen-filled counters. because the mobility of ions in hydrogen is much greater (about ten times) than that in argon, and the recording speed of the pulses of hydrogen filled counters on the oscilloscope screen was too high to photograph with our camera. The observed pulses are quite similar to the theoretical one shown in Fig. 3, and it is very clear from this fact that the pulses are constructed by many small discharges.

In hydrogen-filled counters, the pulses show less fluctuation both in height and in duration, and the investigation of the properties of the pulses is much easier than in argon-filled counters. We measured the pulse heights and the discharge durations of hydrogen-filled counters directly by the naked eyes with a scale drawn on the screen of the oscilloscope for various pressures of the fillings. The accuracy of measurement of the pulse heights and the discharge durations was, however, somewhat poor, because there are still some fluctuations.

Fig. 7 shows some sketched pulses of a hydrogen-filled counter at various voltages. At very low overvoltages, the rising part of a pulse consists of a single step or of several steps, and the durations of each step are nearly the same one with another, and do not strongly depend either on the overvoltage or on the situation in the stair. The durations of each step depend, however, on the pressure of the fillings, as shown in Table 1.

The pulse shapes depend also on the leak resistance and on the capacitance of the wire system, as shown in Fig. 8. With a very low leak resistance, the tops of the pulses become flat and rugged. If the capacitance of the wire system increases, the pulses require longer time to grow up and their rising parts become smooth. In the recovering part of the pulses, the potential decays exponentially

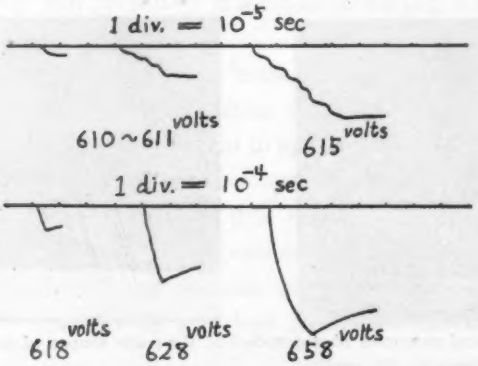

Fig. 7. The pulse shapes sketched of a hydrogen-filled counter at various applied voltages. (Fillings: H, 30 mm Hg)

Filling.	Pressure.	Applied voltage.	Observed duration of each step in the rising parts of the pulses.	Theoretical transit time.
	mmHg	volts	μsec	μsec
Argon (κ=1.4)	100	530	70 ~ 140	215
	29	370	40 ~ 70	90
Hydrogen (κ=13.8)	100	1140	10 ~ 15	10.2
	30	620	4 ~ 7	5.6
	10	470	4 ~ 7	2.5

Table 1

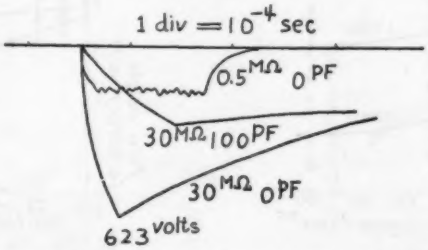

Fig. 8. The pulse shapes for a low leak resistance and for a large capacitance of the wire system. (Filling: H, 30 mmHg, V_0: 623 volts)

and its time constant depends on the leak resistance and on the capacitance of the wire system.

Fig. 9 shows the pulse height and the duration as a function of the applied voltage. The pulse height is nearly proportional to the overvoltage. The discharge duration increases steeply near the threshold, but becomes saturated with increasing overvoltage. With a low leak resistance, sometimes the discharge duration grows suddenly at some value of the overvoltage, and the discharge turns to a

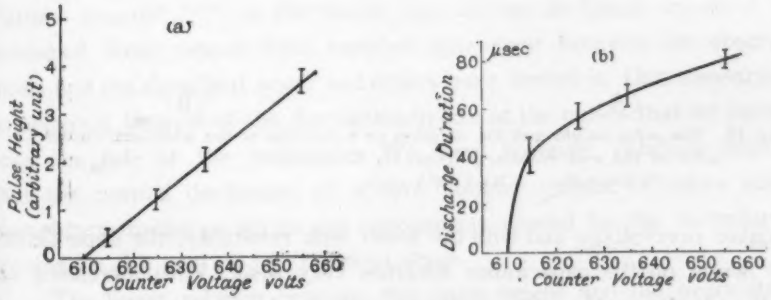

Fig. 9. The pulse height and the duration as a function of the applied voltage. (Filling: H, 30 mmHg)

continuous one.

Fig. 10 show the pulse height and the duration as a funuction of the additional capacitance of the wire system for various leak resistances. The pulse height decreases with increasing capacitance, and this dependence is more remarkable with the heigher leak resistance.

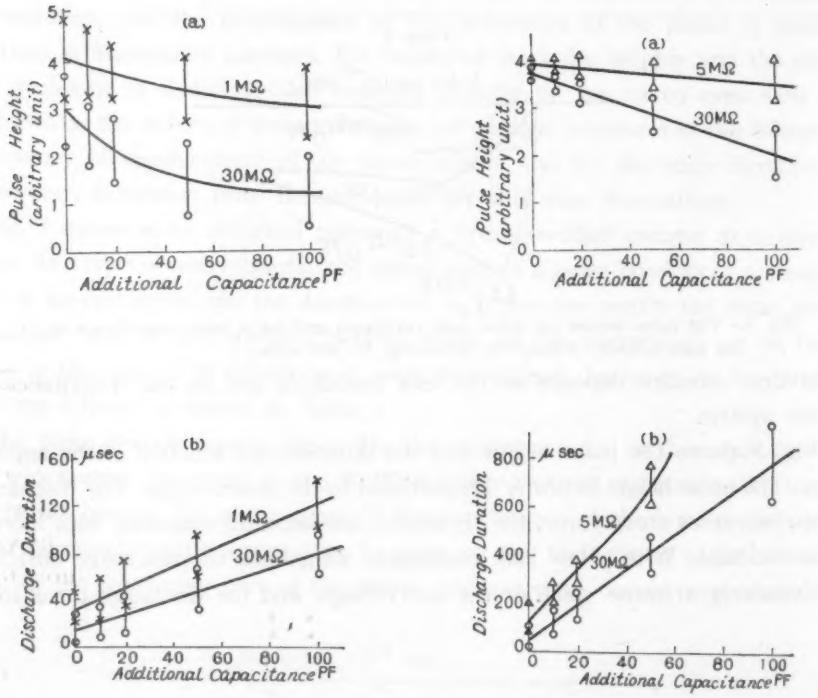

(A) (B)

Fig. 10. The pulse height and the duration as a function of the additional capacitance of the wire system. (Filling: H_2 30 mmHg)
(A) V_0 616 volts, (B) V_0 653 volts.

At the higher overvoltage and with the lower leak resistance, the dependence of the pulse height on the capacitance becomes very weak. With increasing capacitance, the discharge duration increases and its fluctuation becomes greater. With decreasing leak resistance, the fluctuation of the discharge duration becomes also greater.

There is a critical minimum leak resistance for an overvoltage, and the discharge turns to a continuous one with a lower leak resistance than this.

In a high pressure counter, the fluctuation of the pulse height is very remarkable — especially near the threshold, and here the dependence of the pulse height on the capacitance is very strong, as shown in Fig. 11, but the discharge duration does not strongly depend on the capacitance. In general, the dependence of the pulse height on the capacitance becomes weak with the deacresing leak resistance, and the leak resistance can be lower in the higher pressure counter than in the lower pressure one.

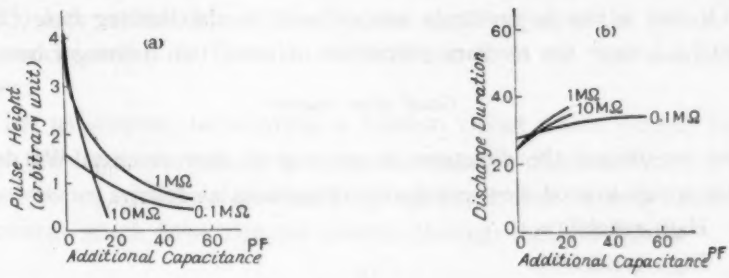

Fig. 11. The pulse height anc the discharge duration as a function of the additional capacitance. (Filling: H, 100 mmHg, V_0: 1140 volts)

7 Discussion

Comparison between the observed results and the theortical expectations

The theoretical transit times of the ions at the same condition with in the experiments are shown in Table 1, and we can see that these transit times are nearly the same with the durations of one step of the stairs of the observed pulses. Various peports[5), 11), 17)] on the transit time of ion in Geiger counters have been published. Some reports have asserted agreement between the observed transit times and the theortical ones, and others have denied it. Our measurment is not so accurate because of the fluctuation in size of the pulses that we cannot support only one side of the contention. We may, however, conclude with assurance that the normal discharges of a slow counter consist of many stages of the elementary discharge which are successively caused by the secondary electrons ejected by the ions of the previous stage.

The linear relation between the pulse height and the overvoltage may be

17) B. Collinge, Proc. Phys. Soc., 63B (1950) 665.

understood as follows: In the limiting case (A), the pulse height is nearly equal to the overvoltage, and, of course, the pulse height has a linear relation to the overvoltage. The effect of the fluctuation is remarkable only for the small overvoltage, and does not strongly affect the pulse height *versus* overvoltage relation.

The relation between the discharge duration and the overvoltage in the limiting case (A) is logarithmic, and it seems to agree roughly with the experimental results, as shown in Fig. 9 b. When the leak resistance is small, or when the external capaditance is large, the duration shows exponential rise, and this is caused from that the discharge is cut off by the fluctuation of the number of the secondary electrons, correrponding to the limiting cases (B).

The pulse height is independent of the additional capacitance in the limiting case (A), and is nearly inversely proportional in the limiting case (B). Figs. (10) and (11) show the medium properties of these two limiting cases.

Good slow counter

Now we discuss the directions to get a good slow counter. We define the properties which a good slow counter must possess as follows:

1) High reliability.
2) High sensitivity.
3) High speed. (Short pulse duration).
4) High pulse height.
5) Uniformity of pulse.

We shall discuss only from the view points of the speed, the pulse height and the uniformity of the pulse, since these properties are related to the pulse shape directly.

Most important point for the improvement of the properties is to minimize the capacitance of the wire system. When the capacitance is very small, the wire potential drops below the threshold voltage in the first step, as we see in Fig. 2 (a), and the discharge is completed only in a single elementary discharge. Such a process has been called *overshoot* by Montgomery[5]. In ordinary counter circuits, however, the external capacitance of the wire system is at least several times larger than the capacitance of the wire itself, and *overshoot* is scarcely observed except when the charge of the ion layer is very large as in a very low pressure counter.

The leak resistance decides the maximum overvoltage, as shown by Eq. (37), but a too high leak resistance is not needed. Furthermore, a high leak resistance increases only the time constant of the circuit, and decreases the maximum counting rate.

In regard to the properties of the filling, it is desirable to have a large η

and a small γ. Large η increases the charge included in an ion sheath, as shown in Eq. (1), and the potential drop in one step also increases. Small γ decreases the probability of the successive discharge, and makes the discharge duration shorter. Large mobility of ion is also desirable, since the discharge duration is inversely proportional to the mobility.

Quenching circuit

Quenching circuits of a slow counter may be divided into two main classes: One is that by a high leak resistance, and the other is that by a univibrator circuit. Neher-Harper, Neher-Pickering and Johnson circuits belong to the former, because these are equivalent to pure leak resistors whose resistance is equal to the grid leak resistance multiplied by the amplification of the circuit, as already discussed in section 6. This can be easily shown in the "ion sheath theory" as follows:

Let us suppose, for example, a Johnson circuit whose vacuum tube is working in the linear portion of its dynamic transfer characteristics; i. e. $(i_p - e_g)$ characteristics with the plate supply voltage fixed; then, when a discharge occurs, the current which flows into the counter through the grid leak is

$$i = \frac{\Delta v}{R},$$

whe Δv is the voltage drop on the grid leak whose resistance is R. Then the drop of the cathode potential of the vacuum tube from that of the placid state is

$$\Delta v \cdot \mu,$$

where μ is the amplification of the circuit. The potential drop of the wire is

$$\Delta V = \Delta v(\mu + 1),$$

and,

$$i = \frac{\Delta V}{R(\mu+1)} \approx \frac{\Delta V}{R\mu},$$

We get, therefore, the following equation in place of Eq. (8).

$$l\frac{dQ}{dt} + C\frac{dV}{dt} = \frac{V_0 - V}{R\mu}, \tag{44}$$

and we can see that a Johnson circuit affects as a multiplication of the leak resistance. This relation is applicable to other circuits. If the capacitance of the wire system is the same, the time constant of the counter circuit can not be reduced by the adoption of a vacuum tube quenching circuit. The effective input capacitance of a vauum tube quenching circuit like Johnson's one is, however, much smaller than that of an ordinary amplifier circuit, because the quenching circuit belongs to a cathode follower.

An univibrator circuit provides a good quenching action, but the pulse shape

is independent of the discharge process of the counter.

Fluctuation in the transit time of ions

We estimate the fluctuation in the transit time under some assumptions as follows:

Here, we consider a single gas-filled counter. Let us assume the collision of ions with molecules to be spherically symmetric and elastic. In this case, we may consider the kinetic energy of an ion after a collisions to be given by $\frac{3}{2}kT$, where k is the Boltzman constant and T is the absolute temperature, because the mass of the ion and that of molecule are the same, and the ion loses half of its surplus kinetic energy at each collision.

The average radial drift of an ion between two successive collisions is given as follows:

$$\delta=\frac{Xe\lambda^2}{2mv^2}, \tag{45}$$

where X is the field strength, e the charge of the ion, m the mass of the ion, λ the mean free path of the ion, and v the velocity after the collision. X and v are given in the following equations:

$$X=\frac{V}{r\ln\frac{b}{a}},$$

$$\frac{1}{2}mv^2=\frac{3}{2}kT,$$

where the other notations are the same as mentioned in the previous sections. The average displacement of an ion in each path by diffusion is

$$\varepsilon=\frac{\lambda}{2} \tag{46}$$

The number of collisions from $r=a$ to $r=r$ is, therefore,

$$N(r)=\int_a^r\frac{dr}{\delta}=\frac{3kT(r^2-a^2)\ln\frac{b}{a}}{eV\lambda^2} \tag{47}$$

The half breadth of the distribution of ions by dffusion can be solved in the same way as the problem of random walk, and is given as follows:

$$B=\sqrt{2}cN^{\frac{1}{2}}\varepsilon, \tag{48}$$

where c is a constant which is equal to 0.477 .... The increment of B in the travel from r to $(r+dr)$ is

$$dB=\frac{c\varepsilon}{\sqrt{2N}}dN=\sqrt{2}c\varepsilon\left\{\frac{3kT\ln\frac{b}{a}}{eV\lambda^2}\right\}^{\frac{1}{2}}\frac{r}{\sqrt{r^2-a^2}}dr.$$

The time required to travel for dB is

$$d\tau=\frac{dB}{\kappa X}=\frac{\sqrt{2}\,c\varepsilon}{\kappa}\left\{\frac{3kT\left(\ln\frac{b}{a}\right)^2}{eV^2\lambda^2}\right\}^{\frac{1}{2}}\frac{r^2dr}{\sqrt{r^2-a^2}},$$

where κ is the mobility of the ion.

The half breadth of the distribution of the transit times of ions is, therefore,

$$\Delta\tau=\int d\tau=\frac{c\varepsilon}{\kappa}\left\{\frac{3kT\left(\ln\frac{b}{a}\right)^2}{2eV^2\lambda^2}\right\}^{\frac{1}{2}}b^2 \tag{49}$$

Since the average transit time of ions τ is $b^2\ln\frac{b}{a}/2\kappa V$, as shown in Eq. (18), the ratio $\Delta\tau/\tau$ is

$$\frac{\Delta\tau}{\tau}=\left\{\frac{3c^2kT\ln\frac{b}{a}}{2eV}\right\}^{\frac{1}{2}} \tag{50}$$

This does not strongly depend on the kind of gas or on the gas pressure, but depends on the change in the counter voltage, and for ordinary counters this value is of the order of $10^{-2}\sim10^{-3}$.

In addition to the statistical fluctuation, the transit times of ions are also scattered by the space charge of the ions, because the ions at the front surface of the ion layer are accelerated more strongly by the field than those at the back surface. This effect depends on the charge of the ion layer and on the constants of the circuit, and increases with increasing applied voltage. At a high overvoltage the effect of the space charge on the transit time may be much greater than that of the statistical fluctuation.

Burning process in an elementary discharge

The process of elementary discharge depends on the filling. In single gas-filled counters, the discharge propagates axially only by photoelectric emission from the cathode, and photoionization in the gas does not play any important role in the discharge propagation, because the main part of the light emitted from Townsend discharge in some gas has not sufficient energy to ionize the same gas.

In mixed gas-filled counters, the discharge can propagate with the help of the photoionization in the gas. The cathodic propagation may also appear in slow counters, and the propagation velocity may be much faster than without the cathode effect.

The burning time depends on the kind of gas, the pressure, and the applied voltage. For the higher pressure fillings, the burning time increases, in general, because both the photoelectric efficiency at the cathode and the mean velocity

of electrons near the wire[5] decrease with increasing pressure.

Continuous discharge

We have denied continuous discharge in ordinary counters, but for extremely high or low pressure filling, continuous discharge may appear. A counter having an extemely high pressure filling has a long burning time in each elementary discharge, and it is unreasonable to neglect it in comparison with the ion transit time.

In hydrogen counters, in fact, the observed pulse shapes show gradual rises at the beginning, even when the counter pressure is several cmHg.

L. Colli, U. Facchini and E. Gatti[18] have found that the argon plus 0.1 % carbon dioxide filled counter whose pressure is 760 mmHg can not be quenched by the ion space charge, because the cathodic propagation of the discharge is slow enough in respect to positive ion drift velocity.

For an extremely low pressure counters, the discharge may also be continuous, because the mean free path of electrons grows with decreasing pressure, and the zone of Townsend discharge spreads to be comparable to the dimension of the counter, and the space charge becomes insufficient to quench the discharge itself. The lower limit of the pressure for normal discharge will be far smaller than the pressure which gives the minimum threshold voltage.

Unstable corona discharge

Werner[2] has shown that the self-sustainig discharge current in a cylindrical counter has a minimum value. He has measured the mean lifetime of the not self-sustaining discharge under this critical current, and concluded that the logarithm of the mean lifetime has a linear relation with the current or the overvoltage.

The mean lifetime of not self-sustaining corona discharge may be interpreted by the "ion sheath theory" as follows:*

The minimum corona current is measured when the leak resistance is negligibley small, and the discharge train is cut off by the fluctuation in the number of the secondary electron as described in the limiting case (B) in section 4.

The discharge duration T is proportional to the exponent of the overvoltage, as shown by Eq. (38), and this agrees with Werner's observation. Let us draw a line of demarcation between a self-sustaining discharge and a not self-sustaining one by the mean lifetime T_m; then the voltage V_m that gives the minimum

* Shade[19] explained the cut-off of discharges in a slow counter by the statistical fluctuation in the photoelectric emissions from the cathode, for he had considered the discharge to be continuous.

18) L. Colli, U. Facchini and E. Gatti, Phys. Rev., **84** (1951) 606; 19) R. Schade, Phys. Zeits., **39** (1938) 908.

corona current is shown as follows:

$$V_m = V_s + \frac{e}{gl\gamma V_s}\ln\left(\frac{T_m}{\tau}\right). \tag{51}$$

The minimum corona current, therefore, is given as

$$i_m = \frac{glV_s(V_m - V_s)}{\tau} = \frac{e}{\tau\gamma}\ln\left(\frac{T_m}{\tau}\right). \tag{52}$$

For an example, let

$$\tau = 10^{-5}\,\text{sec}, \quad \gamma = 10^{-7}, \quad \text{and} \quad T_m = 10^{-1}\,\text{sec};$$

then we get

$$i_m = 1.1 \times 10^{-6}\,\text{amp}.$$

We measured the minimum corona current in some counters whose constructions were the same as those of the counters used in measurements of the pulse shapes. The minimum corona current was of the order of 10^{-6} amp in hydrogen-filled counters, and was of the order of 10^{-7} amp in argon-filled ones. We failed to find any corona current over 10^{-8} amp in an argon-alcohol mixture-filled counter even when the overvoltage was 200 volts. These facts will show that the minimum corona current strongly depends upon the probability of secondary emission, because it is very clear that the probability of secondary emission by ion impact is much larger in argon than that in hydrogen, but becomes negligibly small by addition of alcohol vapor.

The minimum current decreases with decreasing gas pressure, and it seems to be inconsistent with our theory, because τ becomes smaller with decreasing pressure. γ depends, however, on the gas pressure, and increases with the ratio of field strength to pressure at the cathode surface, and such increase of γ with decreasing pressure seems to overcome the effect of the decrease of τ.

8 Conclusion

We have calculated the pulse shape of a slow counter under the assumption that the secondary emission from the cathode by ion impact is only a cause which makes the slow counter discharge successive and makes its pulse shape quite different from that of a fast counter.

The behaviors of the calculated pulses fairly agree with those of the observed pulses, and we may conclude that our assumption is reasonable and that the *ion sheath theoy* is proper for the normal discharges in slow counters.

The conclusions are summarized as follows:

(1) The discharge of a slow counter consists of many stages of the elementary discharge (ion sheath formation) which are well known in a fast counter. One pulse of a slow counter is formed by the whole of an train of the elementary discharges.

(2) The minimum leak resistance, the rise time, the discharge duration and the recovery time of a slow counter can be estimated by our theory.

(3) To minimize the external capacitance of the wire system as much as possible is most important to improve the characteristics of a slow counter.

(4) The main effect of a vacuum tube quenching circuit like Johnson's one is the multiplication of the leak resistance.

(5) The minimum corona current can be explained by the *ion sheath theory*.

The author wishes to expres his sincerest thanks to Professor Yoshio Fujioka, director of the Institute, for his kind suggestions and encouragement upon the present work. He is also indebted to Professor Tatsuoki Miyajima for his many valuable advices and discussions on the theoretical investigation, and to Professor Shoji Kojima for his helpful advices in the course of the experimental studies.

A Cathode-Ray Investigation of Thin Films of Tin, Zinc, and Cadmium Deposited on a Silver Crystal Face

Yasuyoshi WATANABE

Department of Physics, Tokyo University of Education

(Received December 15, 1951)

The structure and orientation of the alloy layer produced by the condensation of tin, zinc, or cadmium onto a silver crystal were studied by means of electron diffraction. The etched surface of a massive single crystal of silver and the oriented silver film formed on mica or sodium chloride crystal served as substrate. The temperature of the substrate during condensation of the metal was varied in wide range. It was found that tin evaporated onto the silver face kept at room temperature arranged itself with a definite orientation, and that, even when standing at room temperature, it changed to the Ag-Sn alloy of closest packed hexagonal lattice so swiftly as can not be expected from the normal diffusion constant. The formation of this alloy was interpreted as due to the diffusion of tin atoms through silver lattice. The diffraction pattern of the grown-up alloy proving the submicroscopic "twin" structure of evaporated silver film was observed simultaneously. Zinc and cadmium gave the results similar from each other, but a little different from that of tin. In these cases, their alloy of closest packed hexagonal lattice or of complex cubic lattice (γ-phase) grew, according to whether the temperature of the substrate was higher or lower. In contrast with the case of Ag-Sn, the γ-phase seemed to be formed by the diffusion of silver atoms through zinc or cadmium.

1 Introduction

Pure metal such as tin, zinc, or cadmium is known to form several kinds of alloy with silver metal in the thermo-equilibrium state, according to their composition and temperature. When these kinds of pure metal are condensed in *vacuo* onto a silver mirror face, diffusion will occur through the substrate-deposit interface, forming an intermediate phase of alloy. Information concerning the crystal system of the alloy as well as its orientation related to the substrate crystal can not of course be obtained directly from the thermal phase-diagram, since the system is not generally in an equilibrium state. With the aim of approaching this information, tin, zinc, or cadmium was thinly evaporated in *vacuo* onto a silver crystal face kept at various definite temperatures and was examined by means of electron diffraction at room temperature. The etched surface of a massive single crystal of silver and the oriented silver film on mica or sodium chloride crystal served as a substrate crystal in the present work. The single crystal or oriented film is preferred to a polycrystalline one, since the alloys grown take definite orientation and the results obtained are simple. When the polycrystalline substrate is used, the alloys produced give ring patterns too diffuse to identify without ambiguity, because the different phases of alloy often have nearly equal

interfacial spacings from each other.

The analogous investigation of evaporated tin and zinc film on a single crystal face of copper has been reported by Kimoto[1] of our institute laboratory.

2 Experimental

Two types of silver substrate were employed: massive single crystal and oriented thin films. The silver metals used were of purity as high as available (99.99 %). The massive single crystal was grown by slow cooling from the melt in the electric furnace. After cutting out the desired face with a fine-toothed saw and smoothing with emery paper, it was etched by concentrated nitric acid, by a mixed solution of chromic acid and sodium sulfate, or by a mixture of equal parts of 5 % potassium cyanide and 5 % ammonium persulfate[2] solution. The crystal was immediately washed in distilled water, rinsed in HCl for a few minutes to remove oxides, washed again in distilled water and finally dried with filter-paper. Then it was transferred to the electron-diffraction camera to record the diffraction patterns. The patterns defined the accurate crystal orientation relative to its surface, whence the surface was adjusted to $(100)_{Ag}$- or $(111)_{Ag}$-plane by further emery-polishing and etching as described above.

The oriented silver fiilms were produced as usual by evaporating silver metals in *vacuo* onto a fresh cleavage of mica or artificial sodium chloride crystal kept at about 300°C. The mean thickness of silver film was estimated to have a variation of 500～1000 Å. The surface of silver film thus formed on the mica was indexed by the (111)-net plane, and that on the sodium chloride crystal by the (001)-plane.

The two types of silver substrate, however, did not seem to give any markedly different results from each other, as will be described later. In addition, the oriented silver film has the advantages that it is free from contamination originating in etching and gives comparatively strong intensity of pattern, though the silver film on NaCl is apt to suffer from moisture[3]. For these reasons, the oriented silver films only were used for the substrate in the case of zinc and cadmium.

On the substrate thus obtained, tin, zinc, or cadmium as pure as available was evaporated in *vacuo* of pressure about 10^{-4} mmHg, the mean thickness of the deposit being estimated to be 300～500 Å each. The temperature of the substrate during condensation of the metal was varied in wide range from sample to sample.

1) S. Kimoto, Science of Light (*Rep. Inst. Opt. Res. Tokyo Edu. Univ.*), **1** (1951) 106; 2) G. W. Johnson, J. App. Phys., **21** (1950) 1058; 3) Y. Watanabe and S. Kimoto, Science of Light, **1** (1951) 37.

3 Results

1) Tin

a) Substrate: *Silver film on mica.* —— Tin was evaporated in *vacuo* onto the silver film kept at room temperature, which oriented with the (111)-plane parallel to the surface of mica. Immediately after the evaporation. the film gave electron diffraction patterns as shown in Figs. 1 (a) and 1 (b), the direction of electron beam being along $[110]_{Ag}$-and $[211]_{Ag}$-azimuth respectively. Both the spots and

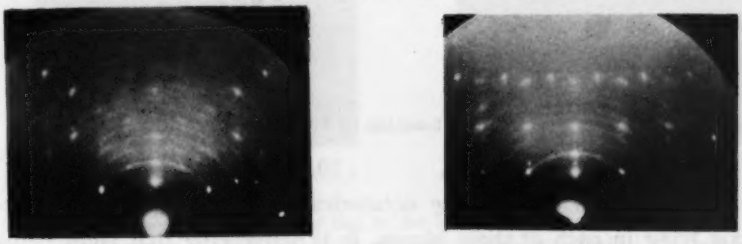

(a) (b)

Fig. 1. Electron diffraction pattern due to the evaporated tin on the (111)-face of silver. In (a) electron beam // $[1\bar{1}0]_{Ag}$-azimuth, and in (b) electron beam // $[2\bar{1}\bar{1}]_{Ag}$-azimuth.

rings in these patterns were identified with those of white tin having a body-centred tetragonal lattice. The orientations of tin crystal with respect to the silver crystal were found to be as follows:

main: $(100)_{Sn} // (111)_{Ag}$, $[010]_{Sn} // [1\bar{1}0]_{Ag}$,

subordinate: $(110)_{Sn} // (001)_{Ag}$, $[\bar{1}12]_{Sn} // [5\bar{1}3]_{Ag}$.

When the sample was left in the dessicator even at room temperature for half a day, it always gave pattern of ε-phase (Ag_3Sn)* superposed on that of tin. The intensity of ε-phase spots distinctly increased with the lapse of time. The pattern of a grown-up ε-phase crystal obtained after the heat-treatment of 200°C for 30 minutes in *vacuo* are reproduced in Figs. 2 (a) and 2 (b). Figs. 3 (a) and 3 (b) are the indexing of Figs. 2 (a) and 2 (b) respectively. The main orientation is interpreted as

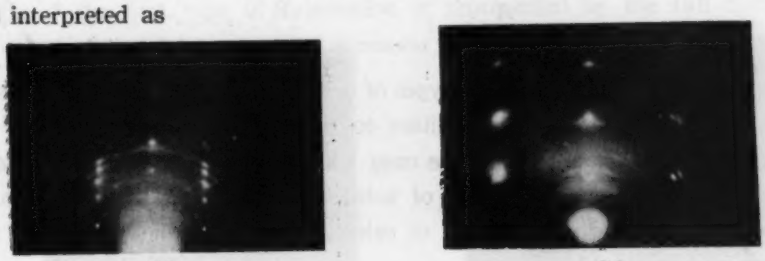

(a) (b)

Fig. 2. Electron diffraction pattern due to ε-phase of Ag-Sn system. In (a) electron beam // $[1\bar{1}0]_{Ag}$-azimuth, and in (b) electron beam // $[2\bar{1}\bar{1}]_{Ag}$-azimuth.

* Highly probable. But this assignment is not absolutely free from ambiguity, because the structure of ε-phase is very close to that of ε'-phase.

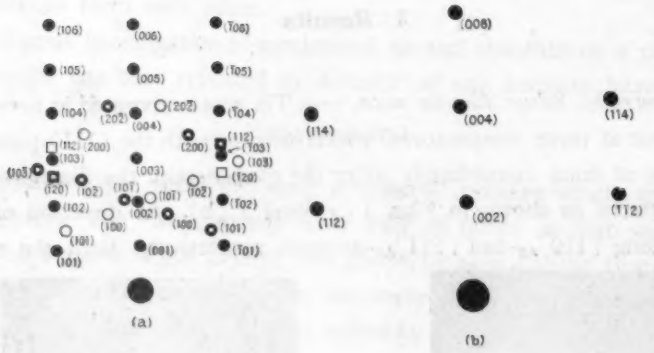

Fig. 3. Indexing of Fig. 2.

$$(00,1)_\varepsilon \,//\, \langle 111\rangle_{Ag}, \qquad [10,0]_\varepsilon \,//\, \langle 1\bar{1}0\rangle_{Ag};$$

where $\langle 111\rangle_{Ag}$ represents each of the octahedral planes, and $\langle 110\rangle_{Ag}$ the corresponding axis lying in each of these planes. It is noteworthy that eight equivalent sets of orientation are all found simultaneously. In this case the silver film employed as substrate has apparent hexagonal symmetry instead of a trigonal one about its surface-normal, or $[111]_{Ag}$-axis, because it was oriented by mica having apparent hexagonal symmetry about its surface-normal when examined by electron diffraction. The silver crystal contains the two types of orientation, the relation between which are schematically shown with A and B in Fig. 4. This fact leads

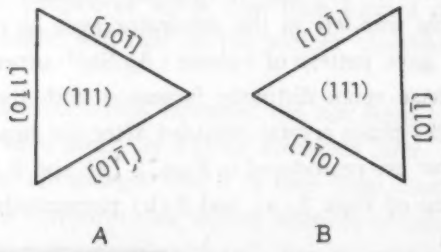

Fig. 4. Schema showing two types of orientation of silver crystal deposited on mica.

naturally to the formation of two types of orientation in the ε-phase, corresponding to A and B. Therefore, in addition to the orientations of $(00,1)_\varepsilon \,//\, \langle 111\rangle_{Ag}$ type described above, are found the ones which are obtained by twinning them on a $(111)_{Ag}$-plane or the surface of substrate. In Fig. 3, the diffraction spots corresponding to the different types of orientation are shown by different marks as follows:

full circles: $(00,1)_\varepsilon \,//\, (111)_{Ag}$ of A or B,
open circles: $(00,1)_\varepsilon \,//\, (\bar{1}\bar{1}1)_{Ag}$ of A,
thick open circles: $(00,1)_\varepsilon \,//\, (\bar{1}\bar{1}1)_{Ag}$ of B.

squares: $(00,1)_s // (1\bar{1}1)_{Ag}$ or $(\bar{1}11)_{Ag}$ of A.

thick squares: $(00,1)_s // (1\bar{1}1)_{Ag}$ or $(\bar{1}11)_{Ag}$ of B.

b) Substrate: *Silver film on sodium chloride crystal.* —— The diffraction patterns obtained immediately after the condensation are reproduced in Fig. 5. The relative orientation was interpreted as

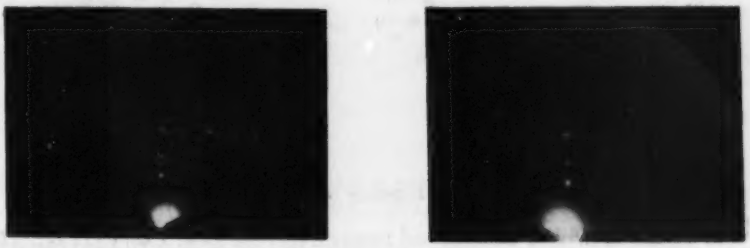

(a) (b)

Fig. 5. Electron diffraction pattern due to the evaporated tin on the (001)-face of silver. In (a) electron beam// $[100]_{Ag}$-azimuth, and in (b) electron beam// $[110]_{Ag}$-azimuth.

main: $(100)_{Sn} // (001)_{Ag}$, $[010]_{Sn} // [100]_{Ag}$,

subordinate: $(110)_{Sn} // (001)_{Ag}$, $[\bar{1}10]_{Sn} // [010]_{Ag}$.

From the findings of cases (a) and (b) it is concluded that the evaporated tin film always grows on silver with its (100) net plane parallel to the surface plane, irrespective of the index of the latter.

In this case again the diffraction pattern changed markedly withe lapse of time even at room temperature. The patterns of a heat-treated sample, corresponding to Figs. 3(a) and 3(b), are shown in Figs. 6(a) and 6(b) respectively. The indexing of them is also shown respectively in Figs. 7(a) and 7(b). Thus there are apparently two types of orientation as follows:

(i) $(00,1)_s // \langle 111 \rangle_{Ag}$, $[10.0]_s // \langle 1\bar{1}0 \rangle_{Ag}$,

(ii) $(00,1)_s // \langle 115 \rangle_{Ag}$, $[10,0]_s // \langle 1\bar{1}0 \rangle_{Ag}$.

In Fig. 7 the first type of orientation is represented by the full circles, open

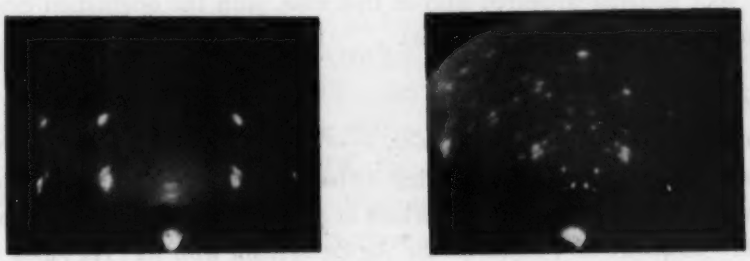

(a) (b)

Fig. 6. Electron diffraction pattern due to ε-phase of Ag-Sn system on NaCl crystal. In (a) electron beam// $[100]_{Ag}$-azimuth, and in (b) electron beam// $[110]_{Ag}$-azimuth.

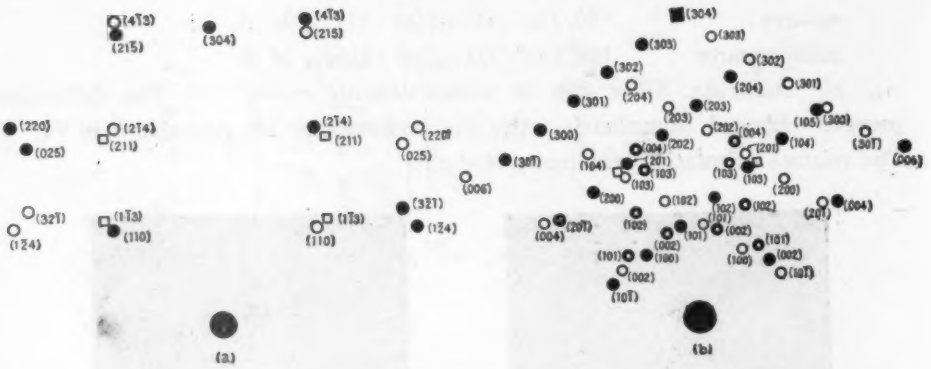

Fig. 7. Indexing of Fig. 6.

circles, and squares, which correspond respectively to $(00,1)_\varepsilon // (111)_{Ag}$, $(00,1)_\varepsilon // (\bar{1}\bar{1}1)_{Ag}$, and $(00,1)_\varepsilon // (1\bar{1}\bar{1})_{Ag}$ or $(\bar{1}11)_{Ag}$ orientations. The second one is shown by thick open circles in the figure. But it must be noted that the latter can be obtained by rotating the former about each $[111]_{Ag}$-axis of original silver crystal by 180° or by twinning the former on each $(111)_{Ag}$-plane. This fact will later be discussed once more.

c) Substrate: *Massive single crystal of silver.* —— Different etchants were found to give different appearances of the etched surface of silver crystal, as observed by means of the microscope as well as by electron diffraction. The surface etched by HNO_3 was rather coarse and thus gave sharp diffraction spots, whereas the one etched by a mixed solution of chromic acid and sodium sulfate or a mixture of equal parts of 5 % potassium cyanide and 5 % ammonium persulfate solution was very smooth and thus gave spots elongated normal to the shadow edge. The patterns obtained after evaporation of tin, however, were found to be quite similar, whichever specimens were used for the substrate.

The evaporated tin patterns were the same as in the film substrate, but only lacked the spots; the tin arranged itself at random on the silver crystal. The ε-phase spot patterns appeared also in this case, with the orientation essentially the same as in the cases (a) and (b).

2) Zinc

a) Substrate: *Silver film on mica.* —— Zinc metal evaporated on this substrate at room temperature gave ring diffraction patterns of itself. When the metal was deposited on the substrate kept at about 110°C, the diffraction patterns gave fibre structure of γ-phase of the Ag-Zn system, with its [110]-axis normal to the surface. When the metal was deposited on the substrate at about 150°C, the diffraction patterns as indexed in Fig. 8 were obtained; i. e., the main part

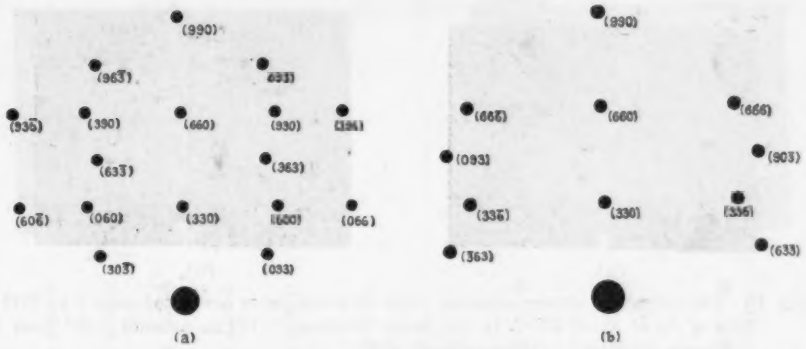

Fig. 8. Indexing of diffraction pattern due to γ-phase. In (a) electron beam // $[1\bar{1}0]_{Ag}$-azimuth, and in (b) electron beam // $[2\bar{1}\bar{1}]_{Ag}$-azimuth.

of the pattern was found to be explained in terms of a single definite orientation of γ-phase. The condensation of metal on the substrate at about 240°C, on the contrary, resulted in the regular growth of the ε-phase, the pattern indexed in Fig. 9.

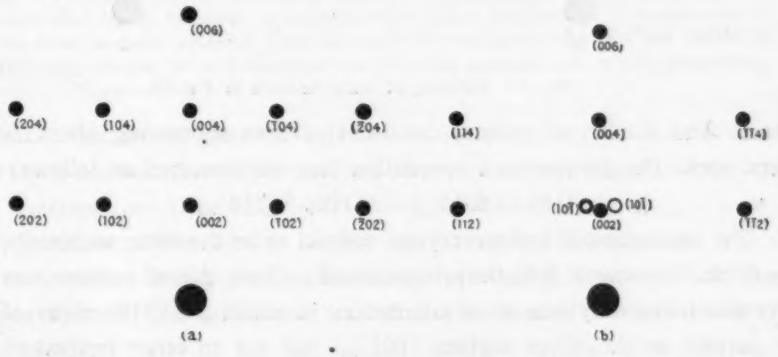

Fig. 9. Indexing of diffraction pattern due to ε-phase. In (a) electron beam // $[1\bar{1}0]_{Ag}$ azimuth, and in (b) electron beam // $[2\bar{1}\bar{1}]_{Ag}$-azimuth.

The two types of orientations are summarized as follows:

ε-phase: $(00,1)_\varepsilon // (111)_{Ag}$, $[10,0]_\varepsilon // [1\bar{1}0]_{Ag}$

γ-phase: $(110)_\gamma // (111)_{Ag}$, $[001]_\gamma // [1\bar{1}0]_{Ag}$.

b) Substrate: *Silver film on NaCl.* —— Zinc metal evaporated on the substrate at room temperature gave ring diffraction patterns of itself. The heat-treatment of the specimen at 200~300°C for about 30 minutes exerted no appreciable effects on the diffraction pattern, whereas the heat-treatment at about 500°C appeared to give the faint patterns of γ-phase superposed on ZnO diffuse rings.

When the metal was deposited at about 200°C, the diffraction patterns as shown in Fig. 10 were obtained. Most of the spots in these patterns were found to be of γ-phase, as is indexed in Fig. 11, but a few of them seemed to be of

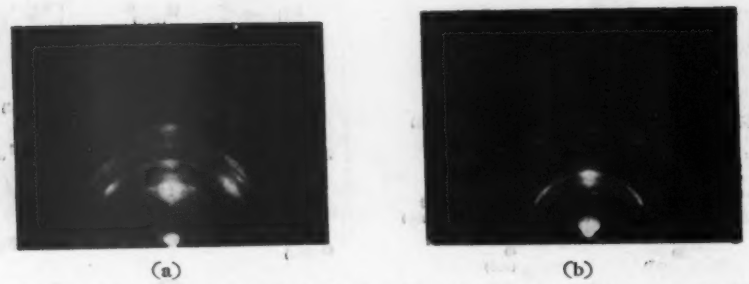

(a) (b)

Fig. 10. The diffraction pattern obtained when Zn metal being condensed onto the (001)—face of Ag at about 200°C. In (a) beam direction // [100]$_{Ag}$-azimuth ±15°, and in (b) beam direction // [110]$_{Ag}$-azimuth ±15°.

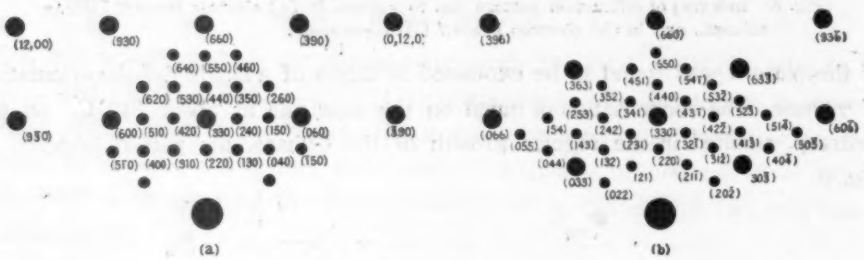

Fig. 11. Indexing of main patterns in Fig. 10.

ε-phase. The pattern of γ-phase consisted of arcs subtending about 30° at the central spot. The predominant orientation may be described as follows:

$$(110)_{\gamma} // (001)_{Ag}, \quad [1\bar{1}2]_{\gamma} // [1\bar{1}0]_{Ag}.$$

The orientation of ε-phase crystal seemed to be the same as described in the case of tin. In contrast with the orientation of ε-phase, that of γ-phase was simpler. There was found only one set of orientation, in which the (110)-plane of γ-phase was parallel to the silver surface $(001)_{Ag}$, but not to other equivalent ones of $\{001\}_{Ag}$.

The specimen mounted on NaCl was apt to suffer from moisture in summer, so that the experiments unfortunately could not be carried out satisfactorily.

3) Cadmium

a) Substrate: *Silver film on mica.*—Cadmium evaporated on the substrate at room temperature gave the diffraction patterns resembling those of Fig. 8; whereas the metal evaporated on the substrate heated above 150° C have the pattern similar to Fig. 9. The orientation of the γ- and the ε-phase related to silver crystal was quite similar to that of the corresponding phase in the case of Zn.

It may be worth noting that the diffraction pattern as illustrated in Fig. 12 was obtained when the temperature of the substrate was relatively high (about 170°C) and Cd was very thinly evaporated. In these figures, patterns of the

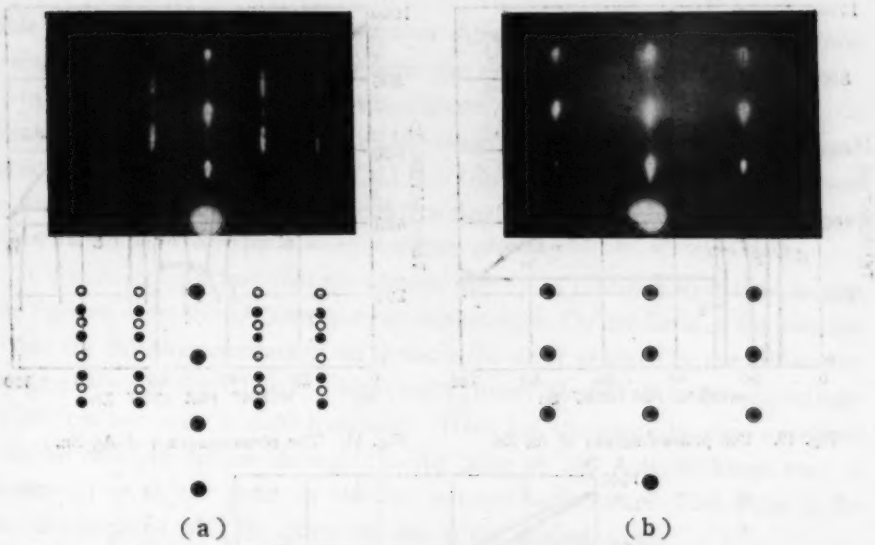

Fig. 12. The diffraction pattern obtained when Cd being evaporated very thinly onto the substrate (Ag-film on mica) at comparatively higher temperature. The spots due to the silver and the grown-up alloy are indicated respectively by dots and circles in the under schema. In (a) beam direction // $[1\bar{1}0]_{Ag}$-azimuth, and in (b) beam direction // $[2\bar{1}\bar{1}]_{Ag}$-azimuth.

closest packed hexagonal type, whose lattice constants are $a=2.88$ Å and $c/a=1.63$, are superposed on the silver pattern. They departed appreciably from the corresponding constants, $a=3.04\sim3.09$ Å and $c/a=1.58\sim1.58$ of ε-phase[4].

b) Substrate: *Silver film on NaCl.* —— Even when the substrate was kept at room temperature during the condensation of the metal, γ-phase of the Ag-Cd system was formed. The orientation was similar to that of γ-phase in the case of Ag-Zn; i. e.,

$$(110)_\gamma // (001)_{Ag}, \qquad [1\bar{1}2]_\gamma // [110]_{Ag}.$$

4 Discussion

The phase-diagrams of Ag-Sn[5], Ag-Zn[6], and Ag-Cd[7] systems are reprinted in Figs. 13, 14 and 15 respectively from the references, where the nomenclatures of the phases employed above, instead of those used in the references, are noted in some cases. ε-phase has a closest packed hexagonal lattice of space group D_{6h}^4, and γ-phase a complex cubic lattice of space lattice T_d^3.

Tin metal deposited on the oriented silver film indicated, as described above,

4) H. Åstrand and A. Westgren, Z. f. anorg. Chem., 175 (1928) 90; 5) A. J. Murphy, J. Inst. Met., 35 (1926) 107; 6) K. W. Andrews, H. E. Davies, W. Hume-Rothery. and C. R. Oswin, Proc. Roy. Soc. (A), 177 (1941) 149; 7) E. A. Owen, J. Rogers and J. C. Cuthrie. J. Inst. Met., 65 (1939) 457.

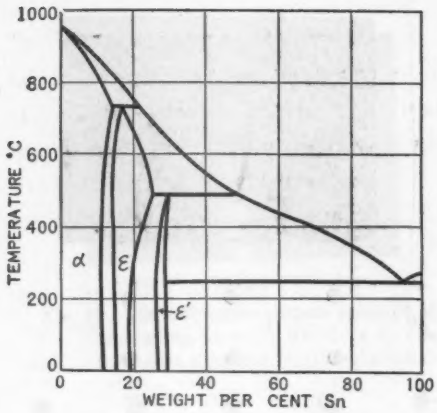

Fig. 13. The phase-diagram of Ag-Zn.

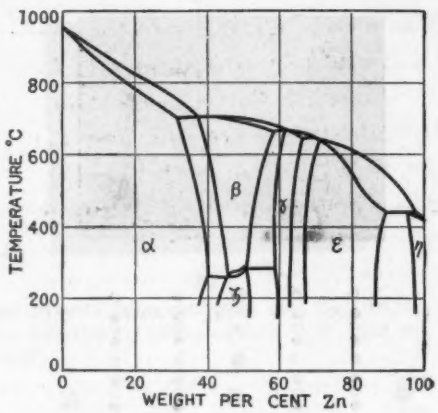

Fig. 14. The phase-diagram of Ag-Sn.

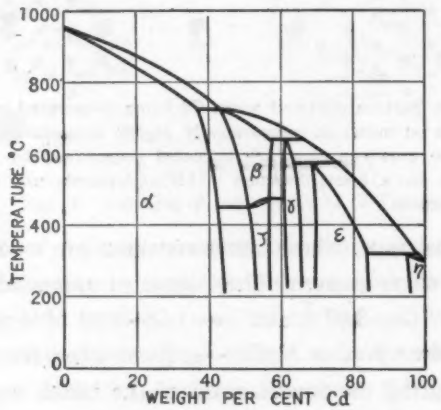

Fig. 15. The phase-diagram of Ag-Cd.

the oriented overgrowth, or epitaxy, but on the massive single crystal surface it did not. The reason for this lack of epitaxy may probably be that the massive single crystal face is covered with oxides.

The orientation was found to develop in such a manner that a basal plane of ε-phase was parallel to each octahedral plane of Ag crystal, and that the relation did not depend upon whether the substrate plane was $(001)_{Ag}$ or $(111)_{Ag}$. Further, in the case of 1) b), it is interesting that the second type of orientation was apparently observed. The silver films employed as substrate in this case were produced by the condensation of silver on the NaCl, and have been supposed to have submicroscopic "twin" structure on their (111)-plane. The second type of orientation can be attributed to the existence of the twin in the original silver crystal. This fact, the writer believes, is a decisive evidence of the twin structure of the evaporated silver film. Further, on the basis of these results. it seems rea-

sonable to conclude that *only the tin atom diffused into the oriented silver crystal* and simultaneously rearranged it to form the ε-phase, but not *vice versa*.

In constrast with the case of tin, γ-phase of both the Ag-Zn and Ag-Cd systems always oriented with their (110)-plane parallel to the substrate surface, irrespective of its index $(001)_{Ag}$ or $(111)_{Ag}$. This fact seems to imply that in these cases the γ-phase contributing to the diffraction patterns is formed by *the diffusion of silver through the oriented zinc or cadmium crystal*.

It was a striking fact that the pattern due to tin changed so swiftly to that of the ε-phase, even though kept at room temperature. On the basis of the assumption that the diffusion constant of tin through the silver is given by the well-known expression $D=D_0e^{-E/RT}$, Barrer[8] empirically found D_0 and E to be respectively 7.9×10^{-3} cm²/sec and 21, 4500 Kcal/atom. Thus, for instance, the time necessary for the Sn atom to diffuse through the Ag layer of 500 Å in thickness may be estimated to be of the order of 10^3 day at room temperature. This value is too large, as compared with the observed one in the present work.

It was found that ε-phase might be formed readily also in the case of Ag-Zn or Ag-Cd. Fig. 12 is of interest in connection with this fact. Miwa and the writer[9] found in their course of study of sulphuration of silver with H_2S gas that the intermetallic compound (Ag_3As) of ε-phase structure was often formed on the surface of silver when the impurity of arsenic compound was not removed from the gas. The patterns obtained by them were very similar to Fig. 12. These patterns seem to imply a "pseudomorphic" structure of the interface.

In the case of tin the diffraction patterns obtained were very clear, but not in the case of zinc and cadmium because of strong background. This background may be due to the relative complexity of the Ag-Zn or Ag-Cd system.

The fact that silver forms the intermediate alloy in contact with active zinc or cadmium is in accord with the findings in electrodeposition of Ag-Cd and Ag-Zn of Nambissan and Allmand[10], Stillwell and Feinberg[11], and Banerjee and Allmand[12], who showed that the deposit produced was not the simple mechanical mixture of metal, but an intermediate alloy.

The results obtained are summarized as follows:

1) When tin was evaporated onto silver, the tin atoms diffused through the silver crystal, but not the silver atoms through tin, resulting in the formation of ε-phase of the Ag-Sn system. The development of ε-phase crystal took place swiftly even when standing at room temperature.

---

8) K. M. Barrer, Proc. Phys. Soc. Lond., 52 (1940) 58; 9) M. Miwa and Y. Watanabe, Proc. Phys. Soc. Japan., 3 (1948) 52: 10) I. Nambissan and A. J. Allmand, Trans. Farad. Soc., 47 (1951) 303; 11) C. W. Stillwell and H. I. Feinberg, J. Amer. Chem. Soc., 55 (1939) 1864: 12) Banerjee and Allmand, Trans. Farad. Soc., 44 (1948) 819.

2) When zinc or cadmium was evaporated on silver, the ε- or γ- phase was formed, according to whether the temperature of the base was higher or lower. The orientation of ε-phase related to the silver crystal is similar to that of ε-phase of Ag-Sn. In contrast with the ε-phase, the γ-phase seemed to be formed mainly by the diffusion of the silver atoms through zinc or cadmium.

3) At the interface of two kinds of metals, such as Ag-Cd and Ag-As, was frequently found a "pseudomorphic" structure of ε-phase.

4) A conclusive evidence was obtained for the submicroscopic "twin" structure on the $(111)_{Ag}$-plane of the evaporated silver film.

5 Acknowledgment

The writer wishes to express his thanks to Professor Mitsuo Miwa for his interest and encouragement during the course of this work; to Mr. Ryoichiro Sato of Taihei metallurgical Laboratory for his contribution of pure cadmium metal; and to Mr. Shizuo Kimoto of the Tokyo University of Education for his preparation of massive single crystals of silver.

Finally, he wishes to record his gratitude to the Department of Education for the financial support.